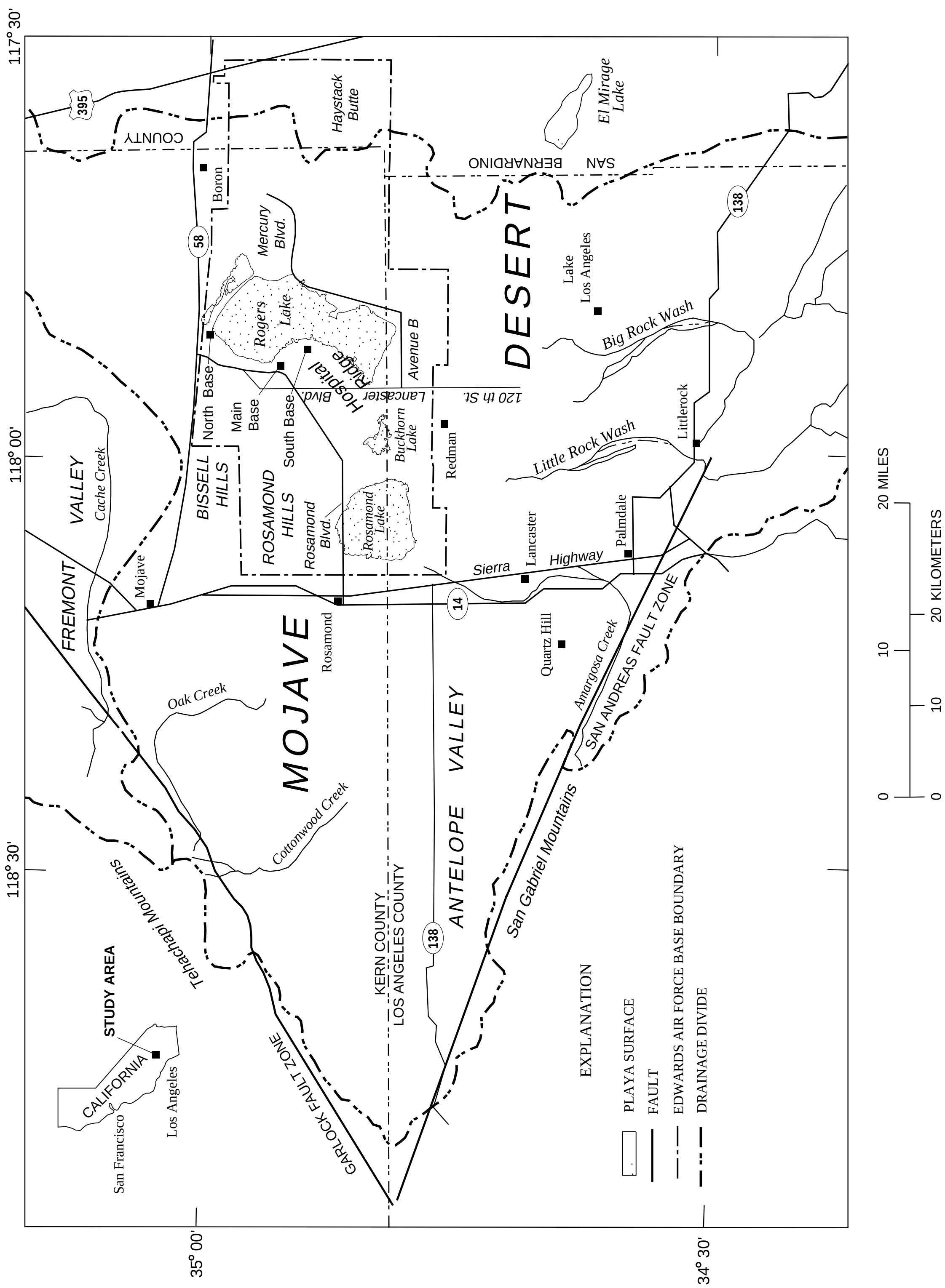

Figure 1. Location of study area.

PWS-0196-0046

LAND SUBSIDENCE AND PROBLEMS AFFECTING LAND USE AT EDWARDS AIR FORCE BASE AND VICINITY, CALIFORNIA, 1990

James C. Blodgett (U.S. Geological Survey, Sacramento, California),

Land subsidence in the Antelope Valley, which includes Edwards Air Force Base, was first reported in the 1950's (Lewis and Miller, 1968); by 1967, about 200 mi^2 of the Antelope Valley were affected by as much as 2 ft of subsidence. Prior to 1973, subsidence on the base was not considered significant. To determine current land-subsidence conditions at Edwards Air Force Base and vicinity (fig. 1), a vertical-control network with 41 bench marks was surveyed in 1989 using the Global Positioning System (GPS); (see Ikehara #1, #2, and Pool #2 abstracts for GPS applications in land subsidence investigations). GPS surveying, described by Collins (1989), is a U.S. Department of Defense satellite-based navigation system designed to provide worldwide positioning capability. Field equipment consisted of roving antenna and receiver-processor units. Precise relative positions of two or more bench marks are determined from satellite-tracking data received simultaneously at each bench mark. This network was developed to provide an area-wide basis for comparing historical changes in bench-mark elevations on the basis of selected stable bench marks. Four stable bench marks that were unaffected by subsidence and with known geoidal heights were used in adjusting the GPS surveys to sea-level datum. Accuracy of the ellipsoidal height for the surveyed area, based on North American Datum 1983 (NAD 83), relative to sea level, is about 0.1 ft (see Ikehara #1 abstract for information on the 1992 GPS resurvey of the Edwards network).

Differential levels to third-order standards of accuracy (National Oceanic Atmospheric Administration, 1980) were surveyed for 65 bench marks in 1989–91 to determine the local distribution of subsidence (fig. 1) and to provide data with which to compare GPS-defined bench-mark elevations. For 14 lines and with lengths from 0.7 to 7.9 mi, the mean difference in bench-mark elevation determined using both methods averaged ±0.05 ft. On Edwards Air Force Base, in the vicinity of Rogers Lake, measured land subsidence ranged from 3.3 ft along the southern edge of the lake to about 0.1 ft on the northern edge (fig. 1). A steady decline of aquifer-system hydraulic heads of more than 90 ft since 1947 measured at a well near Scout Road (fig. 1), is associated with the land subsidence. The amount of land subsidence at the base varies depending on the decline of aquifer hydraulic heads related to ground water pumping from various well fields, and the occurrence of fine-grained compressible sediments in geologic substrata near the zones of ground-water production (Londquist and others, 1993). Near the southern edge of Rogers Lake, the land subsided more than 2 ft between 1961 and 1989 (fig. 2). The average rate of land subsidence near the south end of Rogers Lake for the years 1961–89 is about 0.1 ft/yr (fig. 3).

Land subsidence is causing surface deformation at Edwards Air Force Base and surrounding areas. This deformation has caused the formation of sink-like depressions, earth fissures, and cracks on the playa surface of Rogers Lake. These changes adversely affect the use of the lakebed as a runway for airplanes and space shuttles. Repairs to the lakebed have been unsatisfactory because the load-carrying capacity of the repaired lakebed is less than that of the original lakebed. Continued active surface deformation further adversely affects repairs that have been made to the runways.

The playa surfaces of these ephemeral desert lakes characteristically have smooth, hard, flat surfaces. Some have small (cobblestone size) polygons or large (giant) desiccation polygons whose boundaries are defined by cracks that may be up to several inches in width. The small polygons range from 1 to 4 in. in width; the giant polygons may exceed widths of 300 ft (Neal, 1965). Fissures are a major concern because they may extend to the water table, allowing direct access for contamination by toxic materials. In addition, existing sink-like depressions and associated fissures become avenues of vertical water

PWS-0196-0047

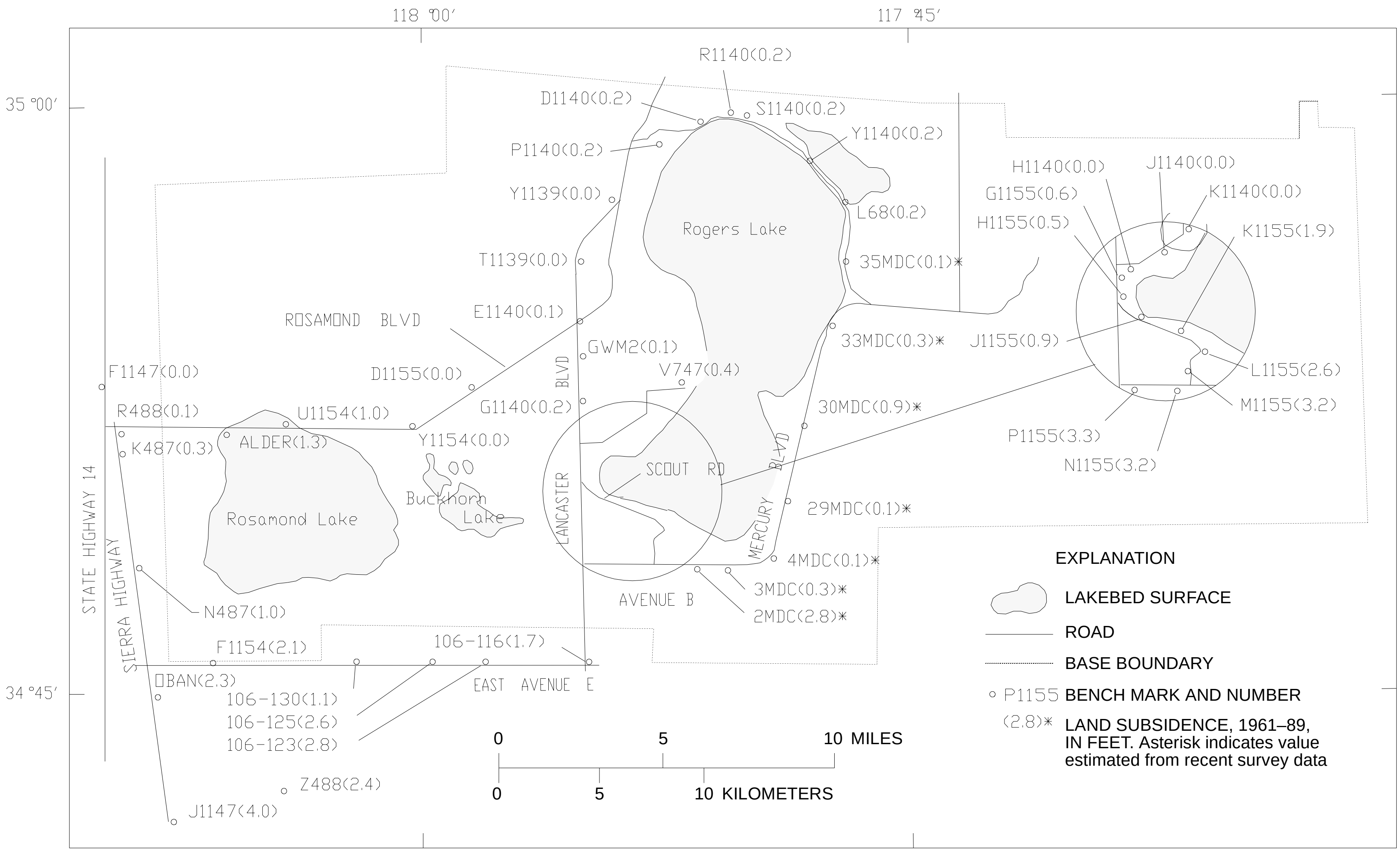

Figure 1. Land subsidence, 1961–89, at selected bench marks at Edwards Air Force Base. Subsidence values are from GPS and differential-leveling surveys.

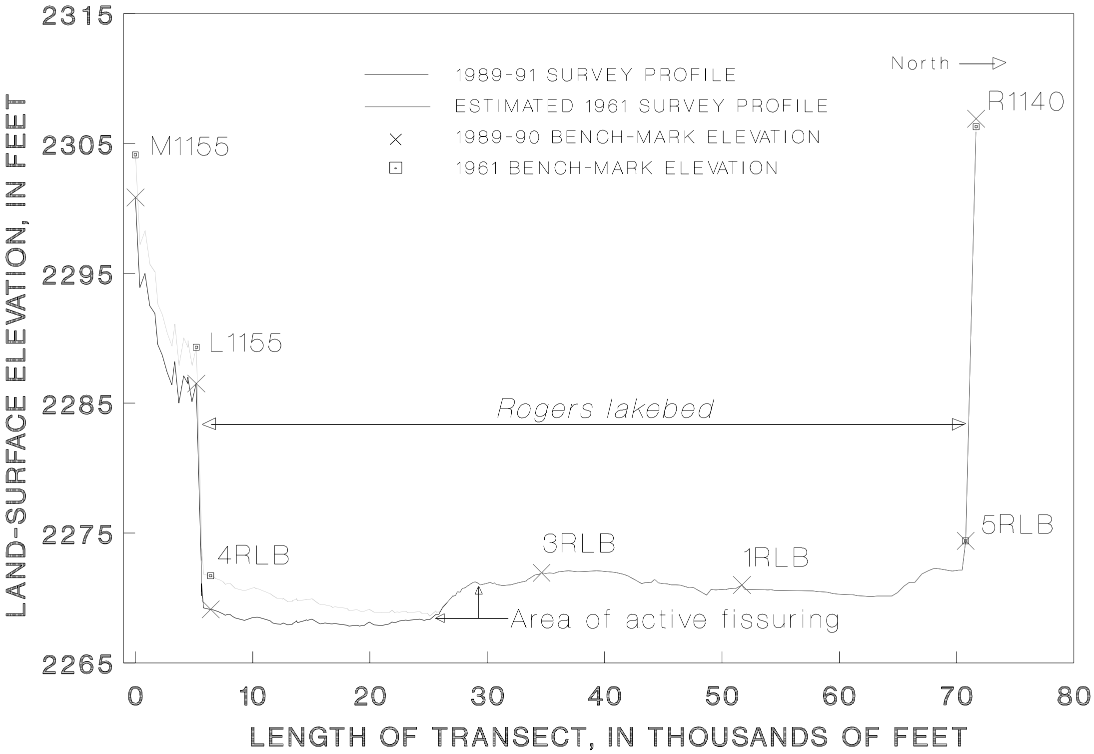

Figure 2. Land-surface elevation, Rogers Lake.

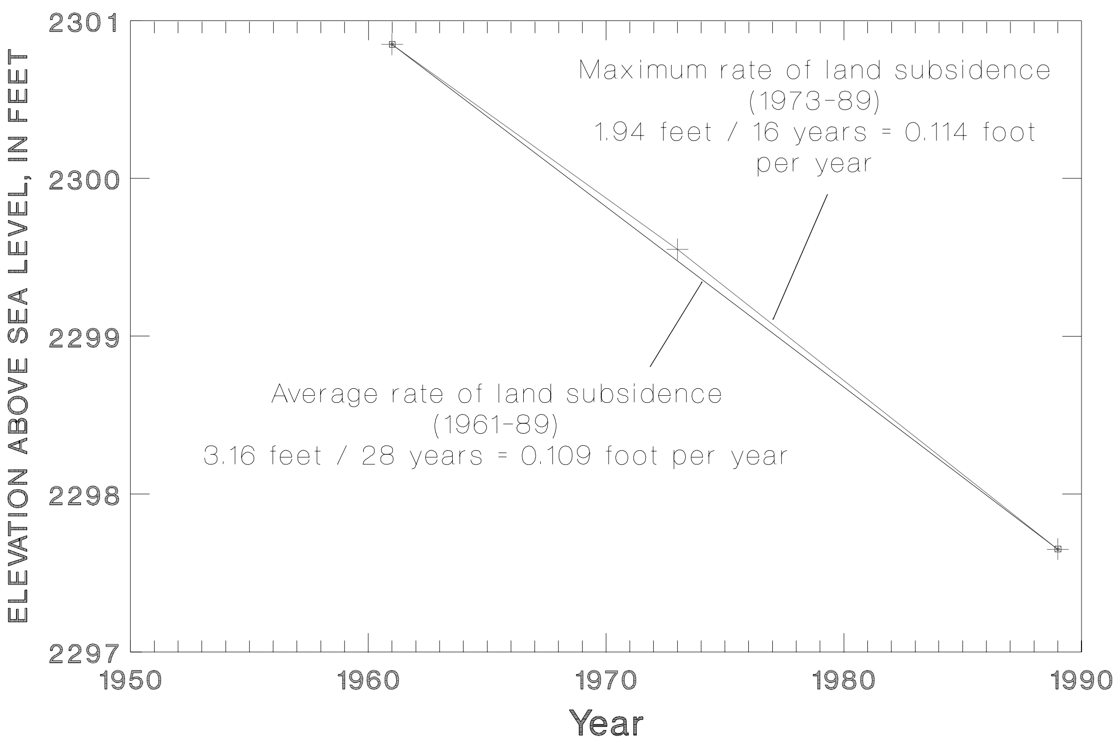

Figure 3. Land subsidence at bench mark M1155 near South Track well field, 1961–89.

PWS-0196-0049

movement. Changes in lakebed slope and land subsidence contribute to the formation of new fissures, and new erosion channels, which form patterns collectively called desert flowers (fig. 4), which increase in size and density following periods of direct precipitation or flooding of the lake. The continued subsidence of the lakebed also has contributed to an increase in the depth and duration of flooding at the south end of Rogers Lake where surface runoff collects in the depression on the lake where subsidence of 2 to 3 ft has occurred.

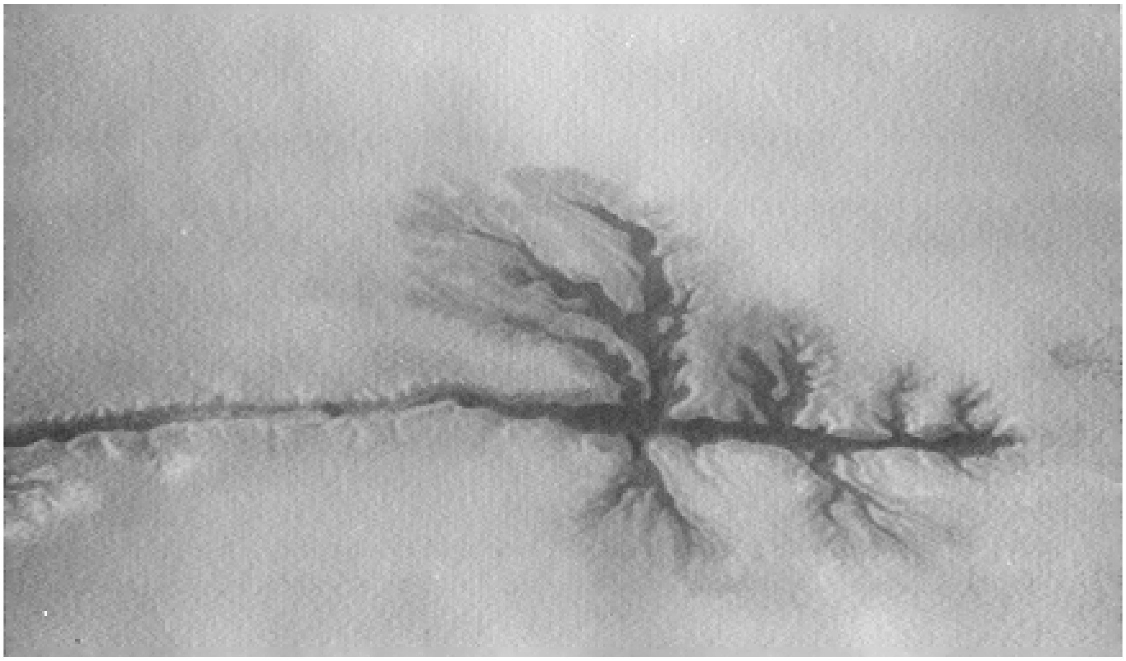

Figure 4. Drainage channels (collectively called desert flowers) caused by erosion during flooding of Rogers Lake. Photographed August 1989.

PWS-0196-0050

LAND SUBSIDENCE AS A RESOURCE MANAGEMENT OBJECTIVE IN ANTELOPE VALLEY, CALIFORNIA

Steven P. Phillips (U.S. Geological Survey, Sacramento, California)

Ground water is an important component of the water supply in Antelope Valley (see Londquist abstract for information on the hydrogeology of Antelope Valley), comprising about 85 percent of the total supply in 1992. Water demand is expected to increase rapidly with the projected increase in population from the current (1994) level of about 310,000 to over 690,000 by the year 2010 (Templin and others, 1994). The combination of about 6.6 ft of land subsidence (4.9 ft from 1961–92; Ikehara and Phillips, 1994) attributable to ground-water withdrawal (Londquist and others, 1993), and the unpredictable nature of surface-water supply, underscores the need for management of Antelope Valley water resources (see Ikehara #1 and Blodgett abstracts for additional information on the measurement of land subsidence in the Antelope Valley).

Although land subsidence is generally considered a negative effect of development, it does have positive attributes. The primary benefit from land subsidence is the water released from compaction of sediments. In some areas of the San Joaquin Valley, it is estimated that as much as 60 percent of ground water applied as irrigation over a 4-year period was derived from compaction (Poland and others, 1975, fig. 42) (see Pool abstract for additional estimates of water derived from compaction in the Picacho Basin, Arizona). Another potential benefit is the creation of a precompacted zone ideal for storage and recovery of surface, imported, or reclaimed water. Water artificially recharged into a precompacted zone can be withdrawn effectively, as heads can be drawn down to their historic low without inducing additional subsidence.

Negative aspects of land subsidence include detrimental effects on man-made structures, geomorphology, ground-water quality, and the hydraulic properties of the aquifer system. Differential subsidence causes tensional forces at the outer boundaries of the subsidence area, and compressional forces at the center (see Helm abstract). Linear engineered structures are particularly susceptible to damage from strain events related to these forces. Canals, sewers, water delivery systems, drainage works, flood-control facilities, transportation grids, well casings, and other engineered structures have all been damaged in subsiding areas (Poland, 1984) (see Schumann abstract for related damages experienced at Luke Air Force Base near Phoenix, Arizona).

Differential land subsidence can affect the geomorphology of an area. Drainage patterns, for example, can be altered substantially by a change or reversal of gradient. Subsidence-related alterations in drainage patterns and local topography can cause severe flooding (see Schumann abstract). Associated problems include increased rates of erosion, as on Rogers Lake, a dry lakebed at Edwards Air Force Base (see Blodgett abstract). Farmland is also susceptible to damage from altered drainage patterns and associated increases in erosion, requiring more frequent grading.

Ground-water quality can be affected by subsidence-related processes. Earth fissures, which are vertically oriented fractures often related to land subsidence, can act as conduits from the surface to the ground-water system. These fissures can provide preferential pathways for the transport of surface or subsurface contaminants to the water table. Another potential effect on ground-water quality is the mixing of relatively poor-quality water from compaction with ground water of better quality. Pore water in clay deposits, which would be released during compaction, is generally higher in dissolved solids than pore water in coarse-grained deposits.

PWS-0196-0051

The hydraulic properties of the aquifer system are also affected by land subsidence. Compaction often results in a permanent loss of storage; most of the loss occurs in the compressible fine-grained units. Compaction also can result in a permanent decrease in the ability of the compacted unit to transmit water. If the fine-grained units are areally extensive and subhorizontal, which is common in alluvial basins of the United States, this could have an effect on the characteristics of vertical flow in the ground-water system.

The optimal management of a water supply generally emphasizes a balance between supply and demand, and a minimization of physical, economic, and environmental consequences. In Antelope Valley and other western basins where land subsidence is occurring, the potential positive and negative consequences of subsidence should be a key management consideration. The experience in Antelope Valley and other semi-arid and arid basins with subsidence shows that land subsidence generally is not included in water-resource management plans. The challenge ahead is to quantify the physical, economic, and environmental effects of subsidence in Antelope Valley and other basins on an areal basis so they can be used in the management process.

DESCRIPTION OF GLOBAL POSITIONING SYSTEM NETWORKS SURVEYED IN CALIFORNIA, 1992

Marti E. Ikehara (U.S. Geological Survey, Sacramento, California)

Three static Global Positioning System (GPS) surveys were completed during 1992 as part of land-subsidence investigations near Mammoth Lakes, and in Antelope Valley, California (see Ikehara #2 and Pool #2 abstracts for GPS applications in land-subsidence investigations). The network near Mammoth Lakes, designed to monitor crustal motion related to subsurface magmatic movement, was modified to include bench marks sited near a geothermal field. Most of the stations of a GPS network established in 1989 at Edwards Air Force Base (EAFB) in Antelope Valley were resurveyed (see Blodgett abstract), and a new GPS network was created and observed in southern and western Antelope Valley.

MAMMOTH NETWORK

An existing GPS network that included the Mammoth Lakes area was densified to obtain information for bench marks within an active geothermal area associated with a resurgent volcanic dome and Long Valley caldera, relative to marks outside the area of geologic unrest (see related abstract by Farrar and others). During a 2-day period, 3 new bench marks were observed simultaneously with 14 stations that are part of the existing Long Valley GPS network (fig. 1). The additional bench marks are Z123 and D916, both of which have been leveled many times, and SRP, a mark newly constructed to establish vertical control for a well used to monitor hydraulic head and subsurface temperature.

All marks were observed with Ashtech Global Positioning System dual-frequency receivers for a period of 6 to 6-1/2 hours. The latitude, longitude, and ellipsoidal heights of the 14 stations were calculated by using fiducial methods, Bernese software, and precise coordinates of the three global tracking stations located in the United States (Jerry Svarc, written commun., U.S. Geological Survey, Menlo Park, CA). The network vectors and geodetic coordinates of the three new stations were calculated with Ashtech postprocessing software. The horizontal coordinates of the existing stations, except for a geographic outlier to the southeast (OVRO), were held fixed to compute geodetic coordinates for the new stations. Marks D916, CONV, and RET had been included in first-order leveling done earlier in 1992 and these elevations were used to define the local vertical control datum (Kenneth Yamashita, oral commun., U.S. Geological Survey, Vancouver, WA.).

A surface gravity map produced in 1992 by the National Geodetic Survey (NGS) shows that gravity measurements used to compute the geoidal separation in the Mammoth Lakes area are coincident with level lines. As a result of this coincidence and the large amount of leveling data over the past decade, the geoid here is well-defined. The GPS-computed elevation and the leveled elevation for Z123 agreed within several millimeters. The error at 1 standard deviation for each of the x, y, and z coordinates measured with GPS was not more than 5 mm.

EDWARDS NETWORK

The primary objective of the GPS survey at EAFB (fig. 2) was to obtain current geodetic measurements of bench marks to aid in the determination of the magnitude and rate of land subsidence in the study area (see related abstracts by Blodgett, and by Londquist). Of the original 41 stations of the GPS

PWS-0196-0053

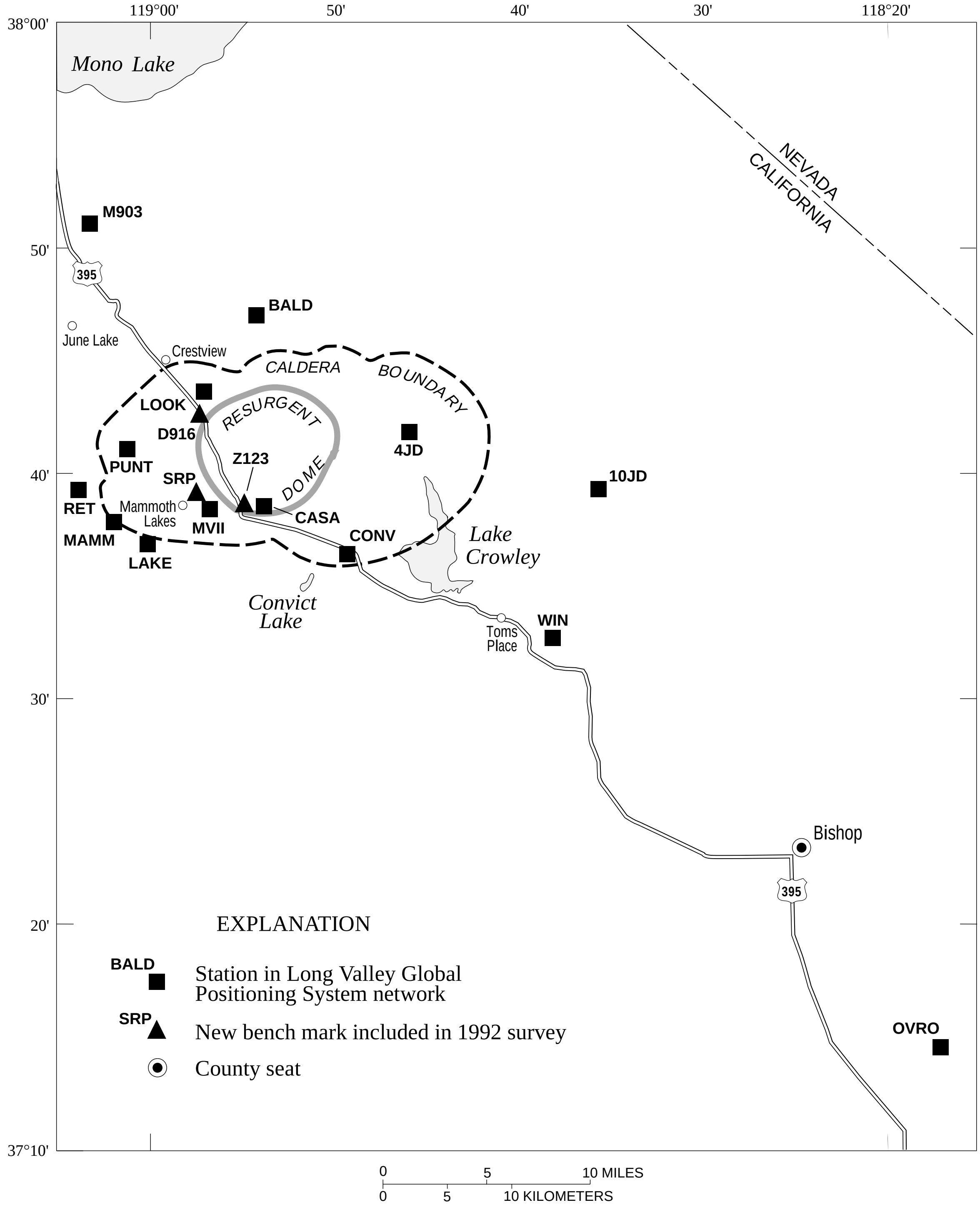

Figure 1. Geodetic control stations monitored by the U.S. Geological Survey for crustal-motion studies in the Long Valley Region, California.

network originally observed in 1989, all but 3 were reobserved in 1992, and 4 new stations were added to the network. Of the 4 new stations, 3 were sited on the perimeter of Rogers Lake to establish vertical control for conventional leveling surveys. The fourth new mark is part of the statewide High Precision Geodetic Network (HPGN).

PWS-0196-0054

Three to five Ashtech GPS dual-frequency receivers were operated daily. Satellites were tracked for a period of 7 hours at most of the stations from mid-March through mid-April. Because Rogers and Rosamond Lakes were flooded until summer, some stations on and adjacent the lakebeds were not occupied until August, when the fieldwork was completed.

The magnitude of land subsidence occurring at EAFB in the past 3 years may not have exceeded the magnitude of the measurement error associated with the vertical component of the 1989 GPS-computed coordinates which is on the order of 3–5 cm. The preliminary error estimate of 1–2 cm for the 1992 survey indicates that the new vertical coordinates provide a more accurate basis for future subsidence comparisons than did the previous survey, which was relatively limited by the older GPS-receiver technology and fewer available satellites in the GPS constellation.

Vector coordinates are related to the local horizontal and vertical datum by holding the positions of geodetic control stations fixed in a network adjustment. Control stations used in the 1989 adjustment will also be fixed in one of the adjustments for 1992 data to produce coordinates that can be examined for changes (exceeding the error), such as those resulting from land subsidence. Another adjustment will be made holding fixed some of the control stations that have been tentatively selected for a regional-scale adjustment of vectors from both the Edwards network and the GPS network newly established in the southwestern part of Antelope Valley.

SOUTHWESTERN ANTELOPE VALLEY NETWORK

A network of bench marks in the part of Antelope Valley south and west of EAFB boundaries (fig. 2) was designed and GPS-surveyed to establish baseline measurements in conjunction with a valley-wide subsidence monitoring program. Increasing demands on ground water and a history of and potential for further land subsidence throughout Antelope Valley have prompted a regional ground-water and land-subsidence investigation. The subsidence-monitoring network may become an integral part of a ground-water (and subsidence) management approach to controlling the location and quantity of ground-water use (see Phillips abstract).

Network stations were selected on the basis of several criteria. The objectives were to extend and tie to the Edwards network, and to include as many Los Angeles County bench marks as possible, particularly those that had a several-decade history of relatively large elevation loss measured by leveling, and those used as control ties between primary level lines established by Los Angeles County. Fifty-two stations, including 10 in common with the Edwards network, comprise the Southwestern Antelope Valley network, which extends from Hi Vista and Llano westward to Gorman (fig. 2). The fieldwork was completed in 3 weeks during April and May with cooperation from Los Angeles County, Department of Public Works. A mixture of Ashtech and Trimble GPS dual-frequency receivers was used and posed little problem during initial postprocessing and vector computation.

Horizontal coordinates of several HPGN stations and possibly a crustal motion network station will be held fixed for horizontal control in a network adjustment. Two of the four bench marks proposed for vertical control are also part of the revised Edwards network control. Network adjustments are being delayed until verification of the new elevation of a bench mark being releveled to a higher degree of accuracy in conjunction with other (non-USGS) GPS surveys. The modeled geoidal separations will be compared with elevations measured by second-order leveling along a 35-km line, completed within a few months after the GPS observations, to determine the magnitude of error associated with the geoid model locally. Vectors from the Edwards network and the Southwestern Antelope Valley network will be combined in a regional adjustment that will use a mixture of control stations observed in each subset of the region-wide Antelope Valley GPS network.

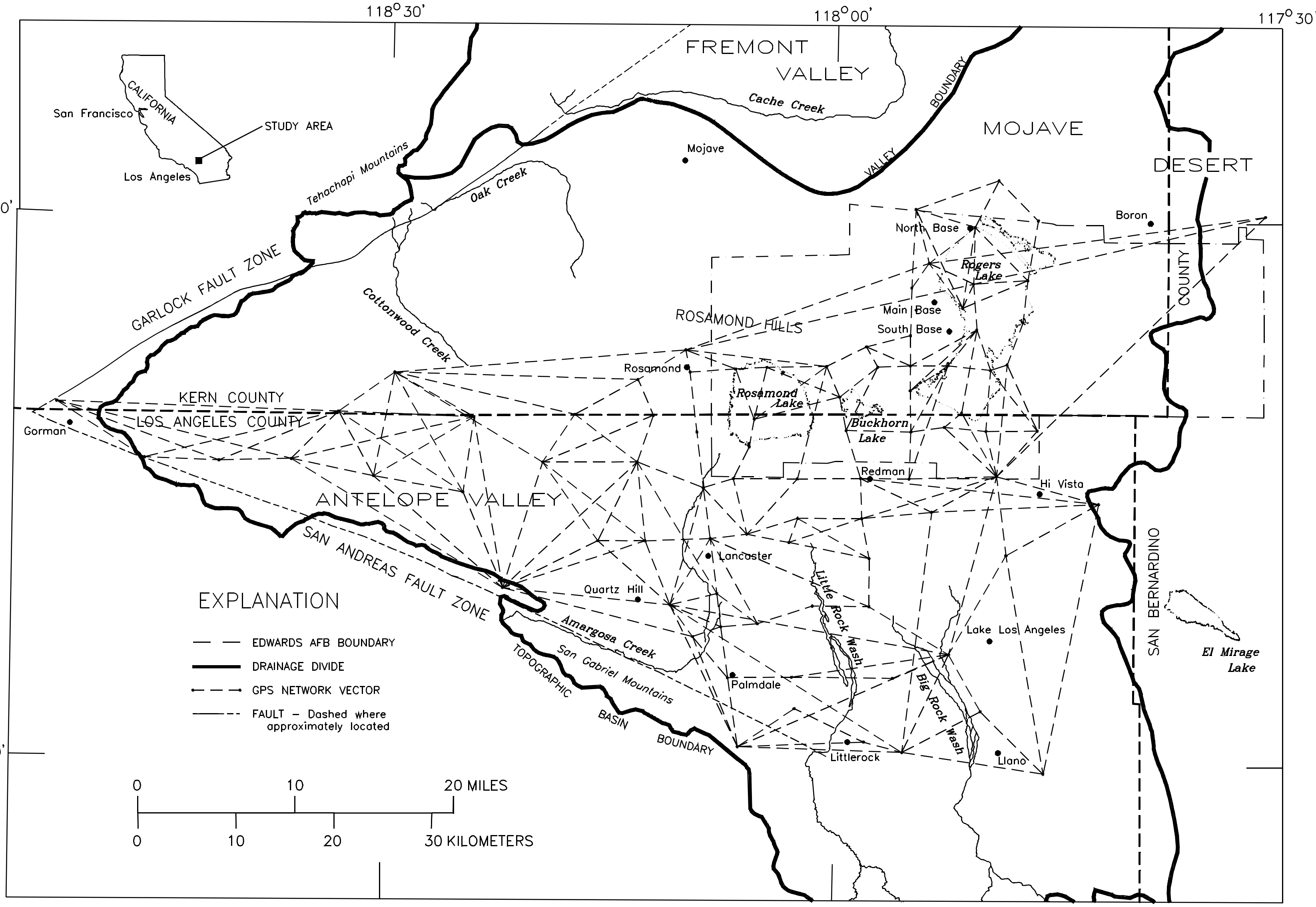

Figure 2. Southwestern Antelope Valley and Edwards Air Force Base Global Positioning System networks.

PWS-0196-0056

STATIC GLOBAL POSITIONING SYSTEM SURVEY DESIGN AND SOURCES OF ERROR IN SUBSIDENCE INVESTIGATIONS

Marti E. Ikehara (U.S. Geological Survey, Sacramento, California)

A Global Positioning System (GPS) survey is most successful when the geometric qualities of the satellite configuration and the receiver network are maximized, and the occurrence and magnitude of systematic and random errors are minimized. By late 1992, there were 21 GPS satellites in 6 orbital planes around Earth, contributing to a period (window) of 7 consecutive hours during which radio signals from 4 or more satellites could be simultaneously observed by receivers. The ideal GPS satellite geometry occurs when the satellites are widely dispersed overhead in each of the 6 orbital planes, throughout the duration of the observation period. The optimal time of day and maximum length of the observation period is dependent on the location of the study area and number of fully operational (healthy) satellites visible at that location.

Designing the pattern of station occupation is a function of the number of receivers available and the amount of redundancy required. For a static GPS survey, the ideal configuration of the loops composed of vectors between stations is circular rather than linear. Vectors should also be relatively similar in length to reduce the sensitivity of the error component of the computed values that is proportional to length. The control stations must be observed a minimum of twice and preferably thrice. Stations most important to the objectives of the GPS survey should also be reobserved. Requirements for different levels of high-precision GPS-survey classifications and detailed guidelines for designing networks to achieve the required level of accuracy can be found in Federal Geodetic Control Committee (1989).

Knowing the speed of radio waves, the distances between several satellites and one receiver can be calculated by timing the interval between transmission and reception of a ranging code carried on the signal. The three-dimensional position of a station on Earth is trilaterated from the knowledge of these distances and of the locations of the satellites within each orbit. The subsidence investigator is primarily interested in the measurement of the vertical position of a station. The ellipsoidal height is the GPS-determined vertical coordinate of a station and is referenced to an ellipsoid, currently Geodetic Reference System (GRS) 80, which approximates the Earth's shape. A closer approximation of the local vertical reference system (datum) is achieved by modeling the difference between the ellipsoid and the geoid, or mean sea level, which is the basis for the vertical datum. Surface gravity and conventional leveling measurements are used to contour the geoidal separations. These relations are expressed by $H = h - N$, where H is the land-surface elevation, referenced to mean sea level, h is the ellipsoidal height, and N is the geoidal separation (fig 1). By convention, when the geoid surface is below the ellipsoid surface, as it is in North America, N is negative. When the land surface is below the geoid (sea level), for example at Death Valley, California, both H and h are negative. When the land surface is above the geoid but below the ellipsoid, H is positive but h is still negative.

For subsidence monitoring, differences in ellipsoidal heights over a period of time at a station can be equated to changes in its vertical position. To compare a station's current vertical position with historic measurements, the geoidal separation, N, must be determined and used to calculate a GPS-derived elevation which is then compared with spirit-leveled elevations. The accuracy of N over the conterminous United States, compared with leveling, ranges from 10-cm root mean square (RMS) at 100-km distances between stations, to 1-cm RMS at 10-km separations (Milbert, 1991a). The inaccuracy of N is the largest source of error in GPS calculations of H.

PWS-0196-0057

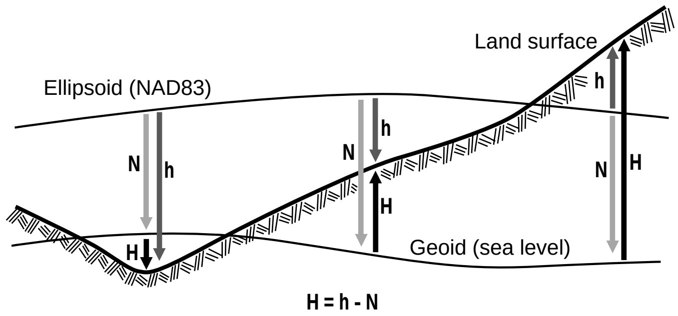

Figure 1. Three possible relations among land-surface elevation, ellipsoidal height, and geoidal separation for a bench mark in North America.

There are two horizontal and two vertical datums currently in use nationally, and there can be local-agency datums as well. The selection of a set of horizontal control stations and a set of vertical control stations (bench marks), each referenced to a single horizontal or vertical datum, respectively, defines the three-dimensional reference system to which GPS vector coordinates are converted. A GPS network for subsidence investigations must have control stations, especially those defining the vertical datum, that are not susceptible to land subsidence. Bench marks suitable for control are those that have been leveled at the same time originally and later show no change in elevation when releveled in several years or decades.

The quality of a set of measurements is defined by its precision, which is the degree of agreement of repeat measurements, and its accuracy, which is the degree of agreement with the true value, the difference of the latter comparison being termed bias. GPS measurements are corrupted by systematic error, which can be either constant in value and thus additive, or proportional, often relative to vector length. Measurements are also subject to random errors that result from variable, usually uncontrollable, observing conditions. Systematic errors are usually minimized by designing a good network and observing schedule. Postprocessing techniques are sometimes effectively used to reduce random errors by correcting or eliminating bad observations.

Although GPS signals are known to bend and slow while traveling through the troposphere (0–10-km altitude), this source of timing error is not significant in the southwestern United States or for vectors less than several tens of kilometers (Dixon, 1991). In environments with low relative humidity, degradation of satellite signals is most severe in the ionosphere (~50–500-km altitude), where ionic activity is proportional to solar radiation. Making GPS observations at night greatly minimizes signal speed corruption resulting from normal atmospheric conditions and the 11-year-cyclical sunspot activity (both systematic error sources) and from extreme solar activity (random error). Because the time delay that radio waves experience when traveling through the ionosphere is frequency dependent, the signals on the L1 (Coarse Acquisition- or Precise(P)-code) and L2 (codeless or P-code) carriers of dual frequency receivers can be compared to estimate the time delay and then correct the calculated distances for ionospheric effects.

Multipathing, another systematic error, occurs when the same signal is detected several times at the antenna after being reflected. This error can be eliminated by choosing locations without reflective surroundings, proper antenna height positioning, and observing for several hours to average out the effect. Additionally, signals below a horizon of 10 to 20º can be filtered out during postprocessing to reduce errors due to both multipathing and atmospheric refraction of low-angle signals.

PWS-0196-0058

Random errors can be resolved only during postprocessing. Noise in the carrier-phase (and rarely in the code-phase) observables, the major random error source, results in cycle slips, interrupting the tabulation of carrier-phase full-wavelength cycles. Cycle slips can be detected graphically and corrected manually. Glitches in signals can result from temporary mechanical failures in satellites, lightning and severe weather or solar activity, and cellular telephone interference. Other random errors result from careless or incorrect execution of field procedures. Differences resulting from imprecise centering and leveling of the antenna over the same station on different occupations are examples of small random errors. An operator error nearly impossible to correct is the incorrect measurement or recording of the height of the instrument, or antenna, above the measurement point of the station.

With careful planning and execution, the horizontal and vertical coordinates of stations in a network can be accurately measured by GPS surveying in support of land-subsidence monitoring.

KINEMATIC GLOBAL POSITIONING SYSTEM SURVEYS IN SOUTHERN ARIZONA

Donald R. Pool (U.S. Geological Survey, Tucson, Arizona)

Kinematic Global Positioning System (GPS) surveys have been used in southern Arizona to quickly obtain accurate altitudes for more than 1,000 well heads, gravity stations, and bench marks and to survey large areas for subsidence distributions. Altitudes are referenced to the National Geodetic Vertical Datum of 1929 (NGVD of 1929). Prior to GPS, altitudes typically were estimated with questionable accuracies from topographic maps because traditional surveys were costly and time consuming. In contrast, kinematic GPS surveys yield altitudes that generally are accurate to 5 cm as long as vector lengths are within about 15 km (see Ikehara #1 and #2 abstracts where for static GPS surveys 1–2 cm level accuracies are expected and achieved).

The survey measures vectors between a static antenna and an antenna that roves among survey points using signals broadcast from military GPS satellites. The static receiver is placed at a bench mark or triangulation station with a known vertical or horizontal position. Vectors to each survey station and geographic position of each station are determined during postprocessing of field data.

Kinematic GPS surveys sacrifice the centimeter-level accuracy of static GPS surveys for greater speed and quantity of positions. Continuous monitoring of a single frequency signal, 19-cm wavelength, from four or more satellites is required. Good satellite geometry is required, which means that the satellites should be spaced across a large area of the sky. Signals from satellites below 13° above the horizon are not used because of excessive noise caused by the atmosphere. In late 1992, 24 satellites are available and surveying can be carried out nearly 24 hours each day.

Surveys must begin with a 10-minute initialization procedure to establish signal bias, which is the number of integer wavelengths between each satellite and the antennas. Signal biases are estimated using baseline or antenna-swap initialization techniques. Baseline initialization requires the remeasurement of a previously measured vector. Antenna-swap initialization requires exchanging the static and roving antennas between two points separated by 5 to 10 m.

The survey consists of roving by vehicle or walking with one antenna and collecting data for 2 to 5 minutes at each station. Some obstructions cannot be avoided while roving, resulting in an interrupted signal. When the signal from a satellite that is essential for good geometry is interrupted, bias on that signal must be reestablished. Often, five or more satellites are monitored and therefore the loss of signal from one satellite does not require reinitialization. When loss of signal results in poor satellite geometry, the signal must be reinitialized by reoccupying a previously measured vector. This vector can be one measured during the same survey, including initialization baseline or antenna-swap point, or one measured during a separate survey.

The typical kinematic survey is impractical in areas with many large trees, developed areas with buildings two or more stories tall, and narrow canyons. Two GPS alternatives, pseudo-static and rapid-static surveys, are available for these areas. The pseudo-static method requires two occupations of 10 minutes for each station but does not require continuous monitoring of satellite signals. The rapid-static method requires a single measurement lasting 20 minutes but is a dual-frequency method that uses more expensive hardware and software.

The typical survey includes 20 or more vector measurements over a 3- to 4-hour period with some redundancy for purposes of error checking (fig. 1). Redundancy is accomplished through inclusion of

PWS-0196-0060

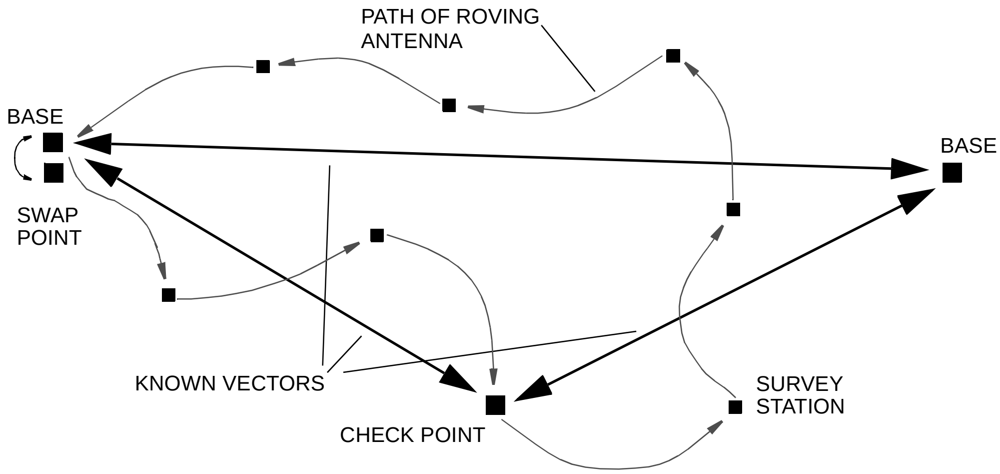

Figure 1. Typical kinematic Global Positioning System survey.

previously measured vectors, repeat measurements, and two base stations. Ideally, one previously measured vector should be remeasured after biases are reestablished on an important satellite signal. Use of two base stations is advantageous because redundancy of positions are provided for each station, power failures or other problems at one base do not cause a total loss of the survey, and poor initializations or mismeasured antenna heights at base stations will be evident from vector-closure errors (see Ikehara #2 abstract for discussion of errors in GPS surveys).

Field data are postprocessed using software from manufacturers of the GPS receivers or the National Geodetic Survey. Basic information necessary for processing include antenna heights and type of initialization. Processing of large surveys can take as much as 45 minutes of computation time. Survey quality can be quickly assessed through inspection of the resulting vectors and comparing repeated measurements. Data can be reprocessed if some of the vectors are suspect or if biases were not accurately estimated. A final fix to recover from unreliable vectors is to remeasure a key vector and then reprocess the data set using the new vector as an initialization baseline.

Processed vectors are loaded into a network-adjustment program and a least-squares adjustment is applied, resulting in the compilation of closure errors and standard errors for each surveyed point. Coordinates of each station in several ellipsoidal coordinate systems can be determined from the known horizontal and vertical positions of base stations.

The final stage of processing is to determine the altitude of each station relative to NGVD of 1929 using the program GEOID90 (Milbert, 1991b). Comparisons of NGVD of 1929 altitudes determined by kinematic methods with the altitude of first-order benchmarks indicate an accuracy better than 10 cm and often better than 5 cm when vector lengths are kept to about 15 km or less.

Kinematic GPS surveys have been a useful tool that has improved the accuracy of altitude-sensitive data and broadened the scope of projects that can be pursued. Accurate well-head altitudes can be measured rapidly and provide more accurate estimates of ground-water gradients. Accurate altitudes increase the accuracy and expand the use of gravity surveys to the detection of small amplitude anomalies that are common in ground-water hydrology. Areas of potential subsidence that have not been surveyed because of cost and time constraints can be easily surveyed. More applications of kinematic surveys are expected in the future.

DEFORMATION ACROSS AND NEAR EARTH FISSURES: MEASUREMENT TECHNIQUES AND RESULTS

Michael C. Carpenter (U.S. Geological Survey, Tucson, Arizona)

Deformation across and near earth fissures is complex and requires varied and extensive instrumentation to determine depth and type of active fissure movement (see Haneberg and Friesen abstract for related discussion of deformation measurements near an earth fissure in New Mexico). Measurements that augment one another include measurements on several different scales, continuous measurements and seasonal repeated surveys (table 1), and combined vertical, horizontal, and tilt measurements.

Table 1. Methods of measurement of horizontal strain.

Method	Approximate range or span, in meters	Approximate resolution	
		Millimeters	Microstrain
Differential Global Positioning System	>30,000	5	2
Electronic distance measurement	>16,000	1	2
Tape extensometry	30	.3	10
Invar-wire extensometer	>30	.001	.03
Pyrex tube and dial gage	3	.0001	.3
Quartz tube and transducer	3	.00001	.003

Precise leveling has a resolution of 0.1 to 0.2 mm or 0.1 microradian for double-run lines as much as 1 km long. Biaxial tiltmeters with AC voltage output for continuous recording have a resolution of 0.1 microradian. Most measured fissure movement has been less than the measurement error for differential Global-Positioning-System (GPS) surveys. Thus, GPS alone is generally inadequate for monitoring fissure movement. However, GPS serves exceptionally well for establishing a fixed frame of reference from which to make the finer measurements.

Three elastic models that explain fissure development and movement are (1) bending of a plate or beam above a horizontal discontinuity in compressibility (Lee and Shen, 1969), (2) dislocation theory representing a fault or tensile crack (Okada, 1985; Holzer and others, 1979; Carpenter, 1993), and (3) upward propagation of tensile strain in response to draping of a material over a horizontal discontinuity in compressibility (Haneberg, 1992; see Haneberg abstract). These three mechanisms probably act together at all earth fissures and are here grouped in the term *generalized differential compaction*. In each case, the horizontal discontinuity can be an edge of a bedrock bench, a mountain-bounding fault, a bedrock high, or a facies change; and, the driving force is differential compaction caused by increased effective stress, which is in turn caused by aquifer-system hydraulic-head decline. The inherent assumption in dislocation modeling is that the differential compaction is concentrated along specific planes such as preexisting faults.

A study was done near Picacho in south-central Arizona from 1980 to 1984 to test hypotheses of earth-fissure movement associated with hydraulic-head fluctuation (see Pool #1 abstract for related land-

PWS-0196-0062

subsidence information for the Picacho Basin, Arizona). Vertical and horizontal displacements were monitored along a single survey line normal to the Picacho earth fissure, while ground-water levels were monitored in shallow and deep piezometers set in each of two test holes on opposite sides of the fissure (fig. 1) and used to compute the aquifer-system hydraulic head. The survey line extends from a bedrock outcrop (fixed reference frame) in the Picacho Mountains on the east, past an observation well near the fissure, to a point 1,422 m to the west. The survey line consists of nine closely spaced monuments (G-O) for tape extensometry and leveling near the fissure and eight widely spaced monuments for electronic distance measurements and leveling elsewhere along the line. From May 1980 to May 1984, the western, downthrown side of the fissure subsided 167 mm and moved 18 mm westward into the basin. Concurrently, the eastern, relatively upthrown side subsided 147 mm and moved 14 mm westward. Thus, the fissure itself translated toward the center of the basin. Dislocation modeling of deformation along the survey line near the fissure suggests that dip-slip movement occurred along a vertical fault surface that extends from the land surface to a depth of about 300 m.

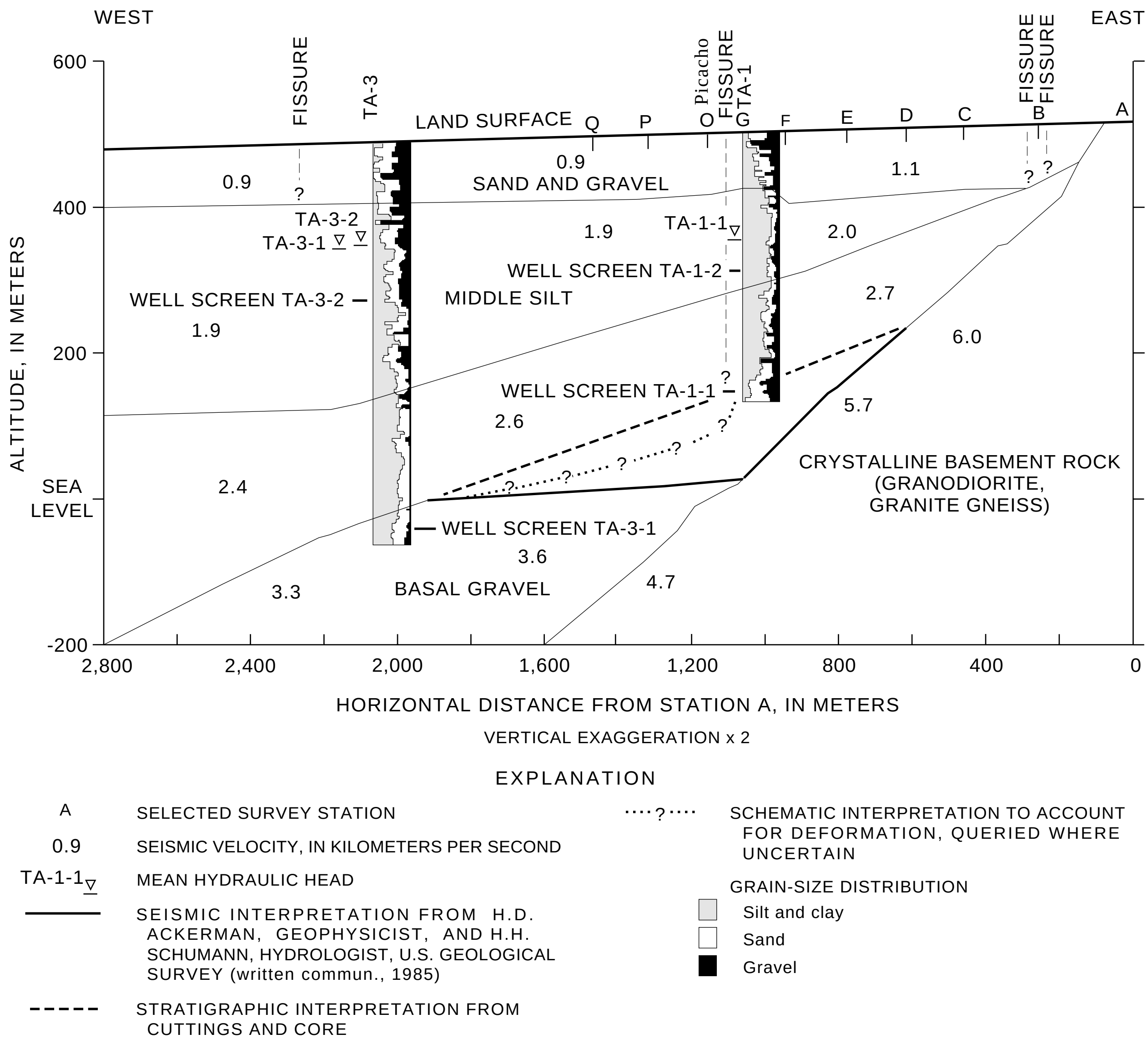

Figure 1. Geologic section constructed from seismic refraction profile and grain-size distribution for test holes TA-1 and TA-3 near Picacho earth fissure.

PWS-0196-0063

Continuous measurements were made of horizontal movement across the fissure using a buried invar-wire horizontal extensometer, while ground-water-level fluctuations were continuously monitored in four piezometers nested in two observation wells (fig. 1). Opening and closing movements of the fissure were smooth and were correlated with aquifer-system hydraulic-head decline and recovery, respectively, measured in the nearby piezometers and with aquifer-system compaction and hydraulic-head fluctuation at Eloy, Arizona, 12 km west in the central part of the basin (see Haneberg and Friesen abstract for related finding for an earth fissure in the Mimbres Basin, New Mexico). Pearson correlation coefficients between the hydraulic-head fluctuations measured in the deeper piezometers, TA-1-1 and TA-3-1, and horizontal movement ranged from 0.913 to 0.925, indicating that differential compaction in the deeper alluvium is the driving force for fissure movement at the study site (fig. 2). The hypothesis of horizontal seepage stresses is not supported at the study site because of the low correlation between fissure movement and horizontal head gradients such as between TA-1-1 and TA-3-1. Correlograms of hydraulic-head decline as ordinate and horizontal strain as abscissa for TA-1-1 and TA-3-1 exhibit hysteresis loops for annual cycles of water-level fluctuation as well as near-vertical excursions for shorter cycles of pumping and recovery, indicating the usefulness of a viscoelastic model such as a Kelvin substance for deformation associated with aquifer-system compaction.

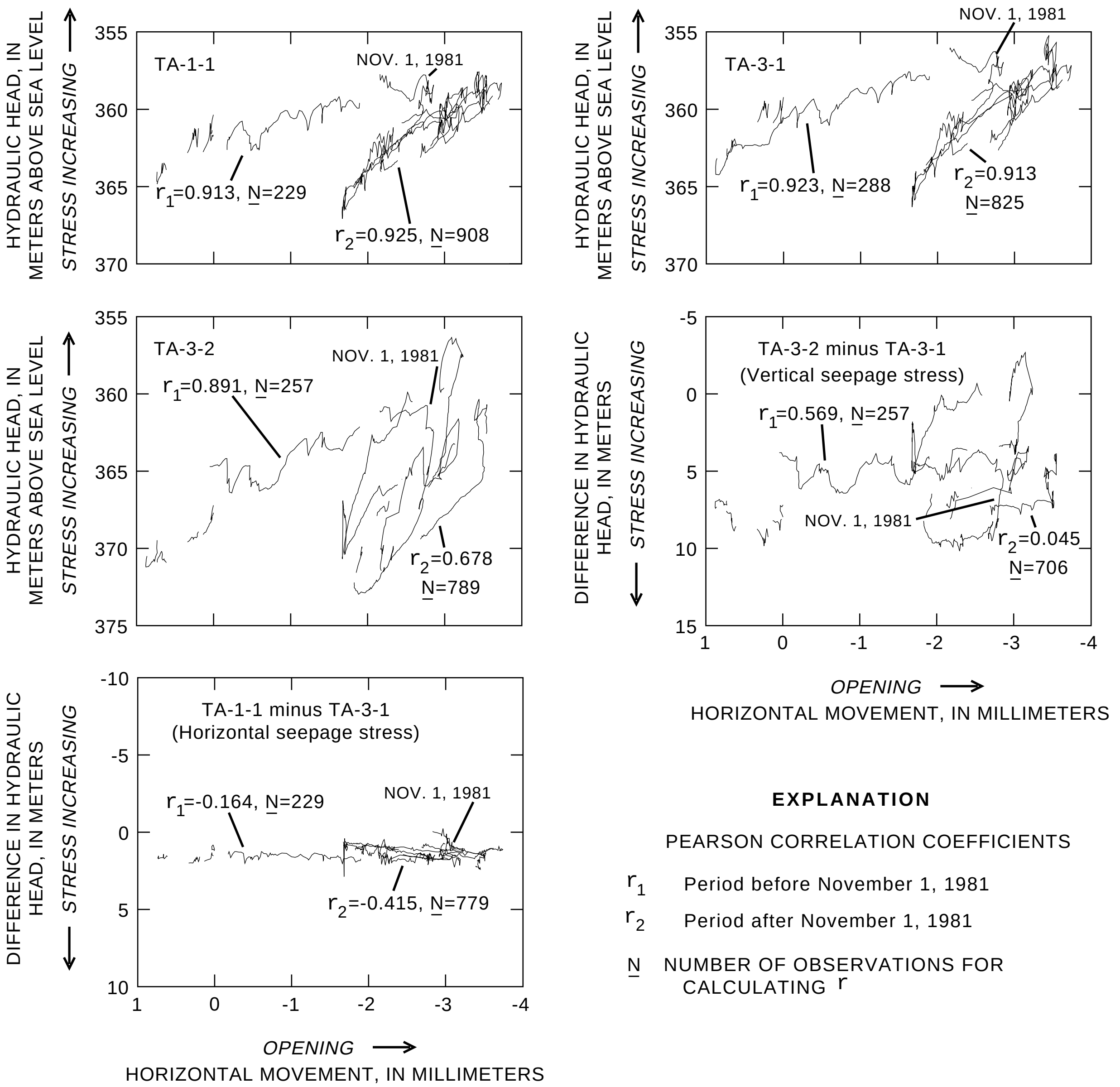

Figure 2. Correlation of horizontal movement with hydraulic-head fluctuations measured in piezometers near the Picacho earth fissure.

PWS-0196-0065

TILT AND AQUIFER HYDRAULIC-HEAD CHANGES NEAR AN EARTH FISSURE IN THE SUBSIDING MIMBRES BASIN, NEW MEXICO

William C. Haneberg (New Mexico Bureau of Mines and Mineral Resources, Socorro, New Mexico), and
Robert L. Friesen (New Mexico Bureau of Mines and Mineral Resources, Socorro, New Mexico)

Earth fissures, related spatially and temporal to basinwide ground-water pumpage and ground-water level declines, occur in at least 13 locations throughout the Mimbres Basin south of Deming, New Mexico. Both the maximum drawdown, in excess of 33 m between 1910 and 1987, and 12 of the fissure locations occur near the center of the 880 km^2 cone of depression in the aquifer potentiometric surface (Contaldo and Mueller, 1991). Subsidence above the center of the cone, estimated from protruding well heads, is believed to be on the order of several decimeters to one meter.

Tilts and ground-water level changes near the Cox earth fissure located in SE/4, SW/4, T25S, R9W were monitored between January and December 1992, using a network of 4 biaxial borehole tiltmeters, 2 piezometers, and a nearby domestic well (fig. 1) instrumented with pressure transducers (Haneberg and Friesen, 1993; Friesen, 1992; see Carpenter abstract for related discussion of deformation measurements near an earth fissure in the Picacho Basin, Arizona). The tiltmeters are sanded into 20-cm-diameter steel casings, so that tilts are averaged over the length of the casing (approximately 2 m for T-A and T-D, and approximately 5 m for T-B and T-C). The objective of this study was to compare observed tilts near the fissure with the deformation patterns predicted by models of simple plane strain draping and differential compaction perpendicular to the trace of the fissure. Previous work at this site included shallow seismic reflection and gravity surveys across the fissure (Haneberg and others, 1991).

The static ground-water levels measured in the piezometers in December 1991 were about 42.6 m below land surface, with a head difference between the piezometers of about 4 cm across the fissure. The depth to water in the piezometers increased approximately 22 cm between December 1991 and late September 1992 (fig. 2)

Resolution of the tiltmeters is 0.1 microradian over a range of $\pm$800 microradian, and resolution of the pressure transducers is 0.013 kPa (the equivalent of about a 1.3 mm height of water) over a range of 0 to 103 kPa (about 0 to 10.6 m height of water). Data were recorded hourly using a digital data logger. Short-term tilt and water-level records exhibit diurnal and semi-diurnal cycles superimposed on long-term trends, with daily tilt amplitudes on the order of $\pm$0.1 microradian and daily water level amplitudes on the order of 1.0 cm. Virtually all of the observed variability can be accounted for by a least-squares regression model incorporating 8 earth tide, barometric, and annual irrigation harmonics, plus a monotonic linear trend (Friesen, 1992; Haneberg and Friesen, 1993; see Galloway abstract for additional information on the analysis of earth tides and atmospheric loading signals in time-series of ground-water level changes). Because a barometer was not available at the field site, however, it is impossible to separate the tidal and barometric components in our data. Recasting tilt values as differential horizontal displacements between the top and bottom of the tiltmeter and assuming zero vertical displacement, we estimate dilation

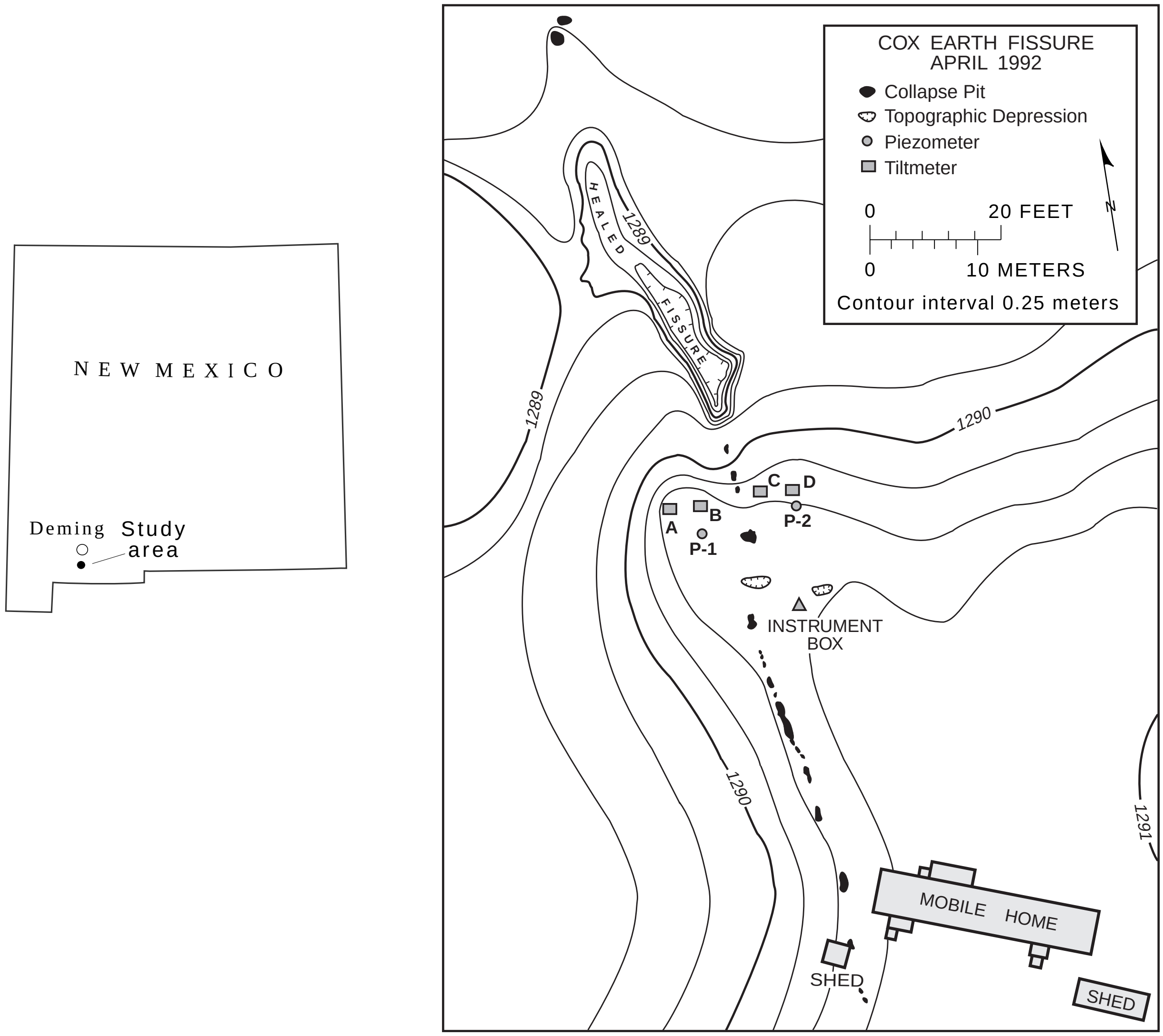

Figure 1. Plane table topographic map of the field site near the Cox earth fissure, showing the trace of the fissure; tiltmeters A, B, C, and D; and piezometers P-1 and P-2. The topographic ridge running through the site is believed to be the surficial expression of a buried channel deposit interpreted on shallow seismic reflection profiles (Haneberg and others, 1991). Tiltmeters T-A and T-D are approximately 2 m deep, and tiltmeters T-B and T-C are approximately 5 m deep.

associated with the diurnal fluctuations to be on the order of 0.01 microstrain, which is the same order of magnitude commonly associated with earth-tide deformation (Bredehoeft, 1967). Daily water level maxima generally correspond to daily tilt maxima, and suggest that the fissure closes as water level rises (see Carpenter abstract for related finding). Because of complicated wave forms, however, we can only speculate that the fissure must open slightly as the water level drops.

PWS-0196-0067

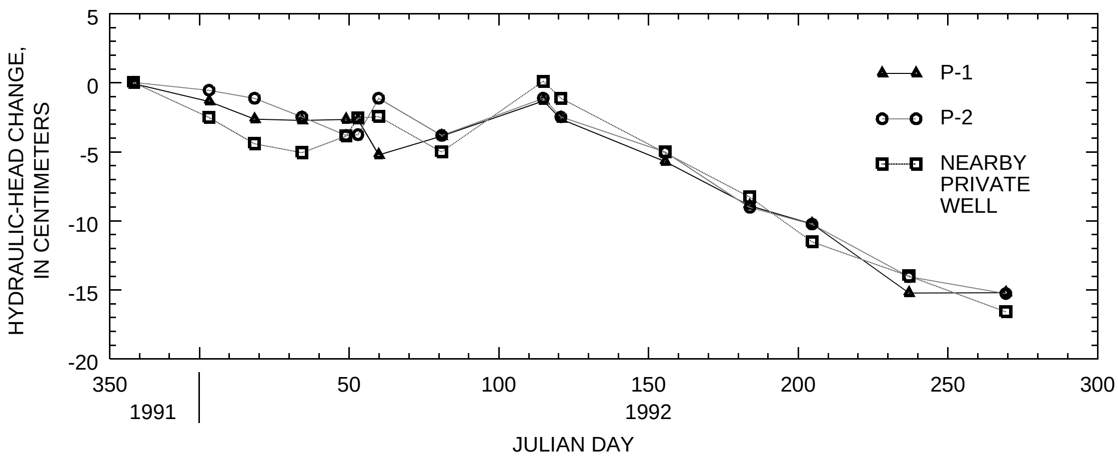

Figure 2. Hydraulic-head changes measured at two piezometers and a nearby domestic well at the field site between December 1991 and September 1992 (Haneberg and Friesen, 1993; Friesen, 1992). Locations of piezometers P-1 and P-2 are shown in figure 1.

Long-term records (tens to hundreds of days) show complicated patterns of tilt both towards and away from the fissure (fig. 3)These patterns are inconsistent with the notion of simple plane strain perpendicular to the fissure, and tilt measurements are only weakly correlated with long-term changes in water level near the fissure. Tilts calculated using a model of a thin elastic plate subjected to spatially-variable loading, for example due to differential compaction over the buried channel deposit beneath the site (see Haneberg abstract), lead us to speculate that highly variable tilts may be caused by flexure of surficial layers over buried stratigraphic and structural irregularities above the water table (Haneberg and Friesen, 1993).

PWS-0196-0068

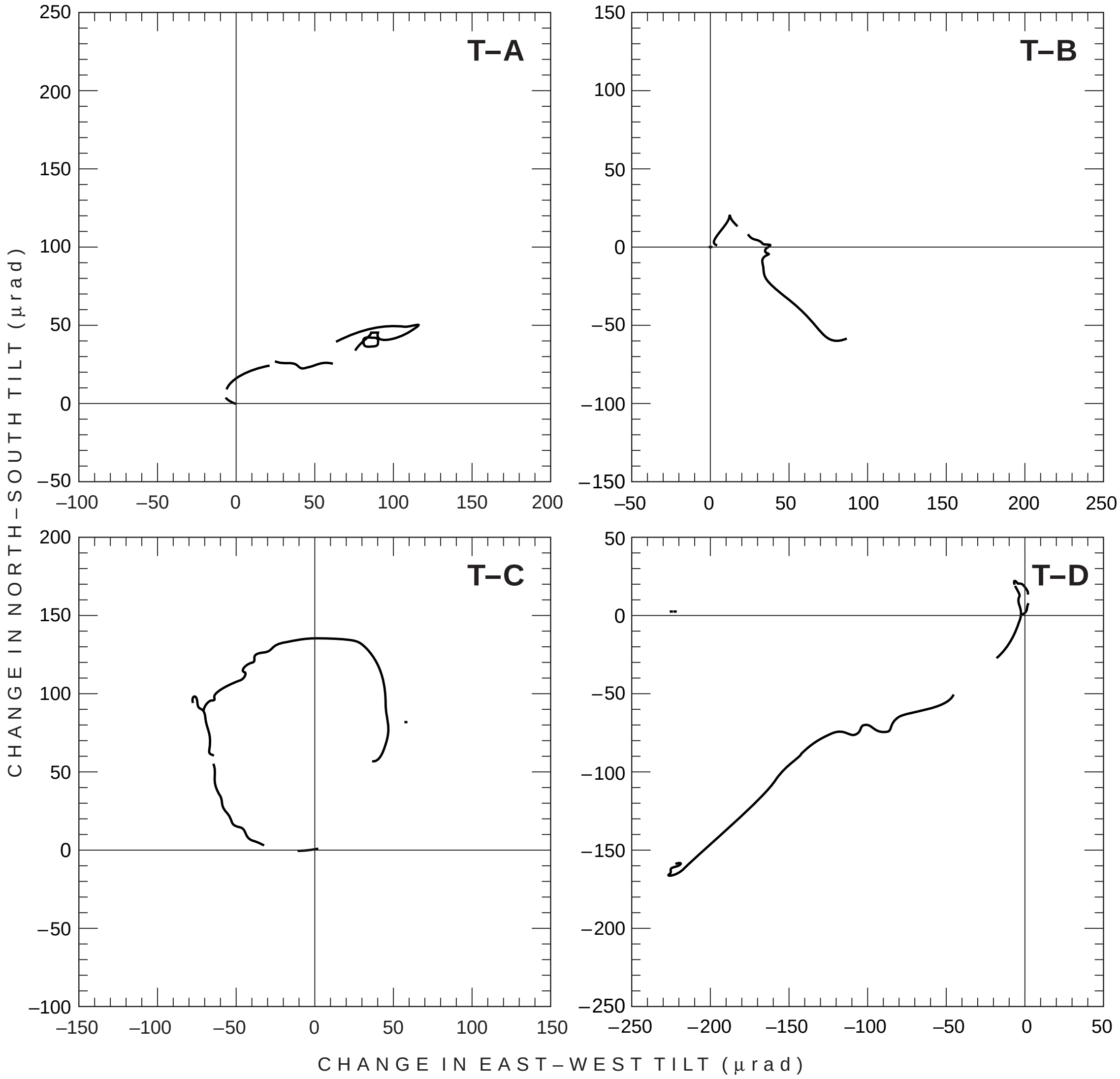

Figure 3. Plan views of data obtained from tiltmeters T-A, T-B, T-C, and T-D near the Cox earth fissure between mid-January and late September 1992. Instrument locations are shown in figure 1. Although the E-W and N-S ranges are the same magnitude for individual tiltmeter plots, the ranges vary among plots according to the amount of tilt measured. During the period of record, tiltmeter A tilted down towards the northeast, tiltmeter B tilted down towards the southeast, tiltmeter C tilted down towards the northeast, and tiltmeter D tilted down towards the southwest.

PWS-0196-0069

CONTINUUM SOLUTIONS FOR DRAPING AND DIFFERENTIAL COMPACTION OF COMPRESSIBLE ELASTIC LAYERS—IMPLICATIONS FOR THE ORIGIN AND GROWTH OF EARTH FISSURES

William C. Haneberg (New Mexico Bureau of Mines and Mineral Resources, Socorro, New Mexico)

In order to investigate the relation between draping of compressible surficial layers over buried irregularities and zones of ground failure (Holzer, 1984; Helm, 1992), continuum solutions have been developed to model the deformation both of single- and multiple-layered elastic bodies subjected to vertical displacement of the lower boundary (Haneberg, 1992, 1993). The geometry and boundary conditions for a single layer model are illustrated in figure 1. These solutions are limited to originally flat, homogeneous, and isotropic elastic layers subjected to lower boundary displacements that can be specified using a Fourier sine or cosine series. The upper surface of the layer(s) is traction-free, corresponding to the Earth's surface. Although the new solutions are not as versatile as finite element solutions previously used to model deformation associated with earth fissures, for example by Jachens and Holzer (1979) and Larson and Péwé (1986), they are simple to program and can be easily implemented on small desktop computers. In the multiple layer model, each layer must also be of constant thickness, although thickness is allowed to vary among layers. Because the new solutions are adapted from the analytic theory of folding, they yield continuous values for stress and displacement throughout the layer, as opposed to the discrete nodal values obtained from finite element solutions. Linear elastic rheology is assumed, so that lithostatic normal stresses can simply be added to the series solutions for perturbed stresses developed as a consequence of draping.

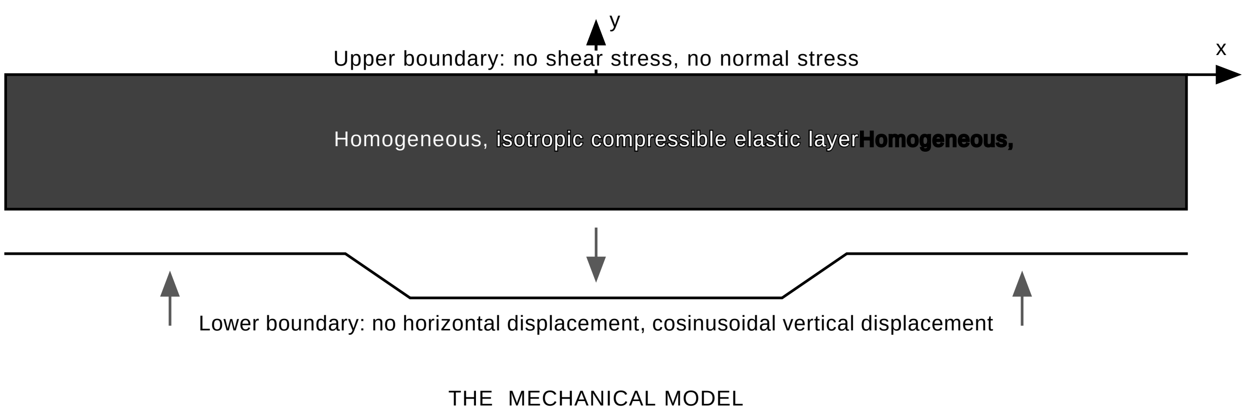

Figure 1. Boundary conditions and geometry of the idealized draping problem. The coordinate system used here is a variation of the system used in Haneberg (1992, 1993), in which the origin is centered over the left-dipping step; this coordinate shift involves only a switch of sine and cosine terms in the published solutions.

Qualitative analysis of the continuum solutions shows that stress and displacement fields developed as a consequence of draping are controlled by: (1) thickness of the layer(s); (2) width of the buried irregularity; (3) amplitude or height of the buried irregularity; (4) stiffness, and to a lesser degree compressibility, of the layer(s); and (5) the shear strength of the lower boundary. The issue of lower boundary shear strength arose during an analysis of tectonic drape folds in sedimentary strata (Haneberg, 1992), and is probably not important in shallow unconsolidated layers.

PWS-0196-0070

A series of numerical experiments with the single layer model yields results that may have implications for the origin of earth fissures (figs. 2 and 3). Zones of high stress along the upper boundary correspond to the locations of inflection points along the lower boundary, with tensile stresses developed above convex-upward inflections and compressive stresses developed above concave-upward inflections. If the layer is draped over a broad, low amplitude irregularity, for example a buried channel-fill deposit, tensile stresses are developed only along the upper surface because the confining lithostatic pressure is greater in magnitude than any tension developed at depth. If the irregularity is sufficiently narrow and the layer is sufficiently thin, perhaps corresponding to a buried fault scarp, the model predicts that tensile stresses developed at depth—even in the presence of compressive lithostatic stresses—can be greater than those developed along the ground surface. A narrow step also has the effect of concentrating displacement gradients (i.e., strains) into a narrower zone of larger gradients just above the step.

Because the deposits in which fissures form have little tensile strength, the development of tension at depth means that opening mode cracks may in theory nucleate at the toe of a narrow irregularity and propagate upwards. A propagating opening mode crack will remain perpendicular to the least compressive principal stress in order to maximize the dissipation of strain energy; therefore, an opening mode crack that begins at depth and grows upward will tend to curve away from the irregularity. This phenomenon may explain the location of an earth fissure near San Marcial, New Mexico, that appears to have breached the surface in alluvium above the hanging wall of a small graben-bounding fault (Haneberg and others, 1991).

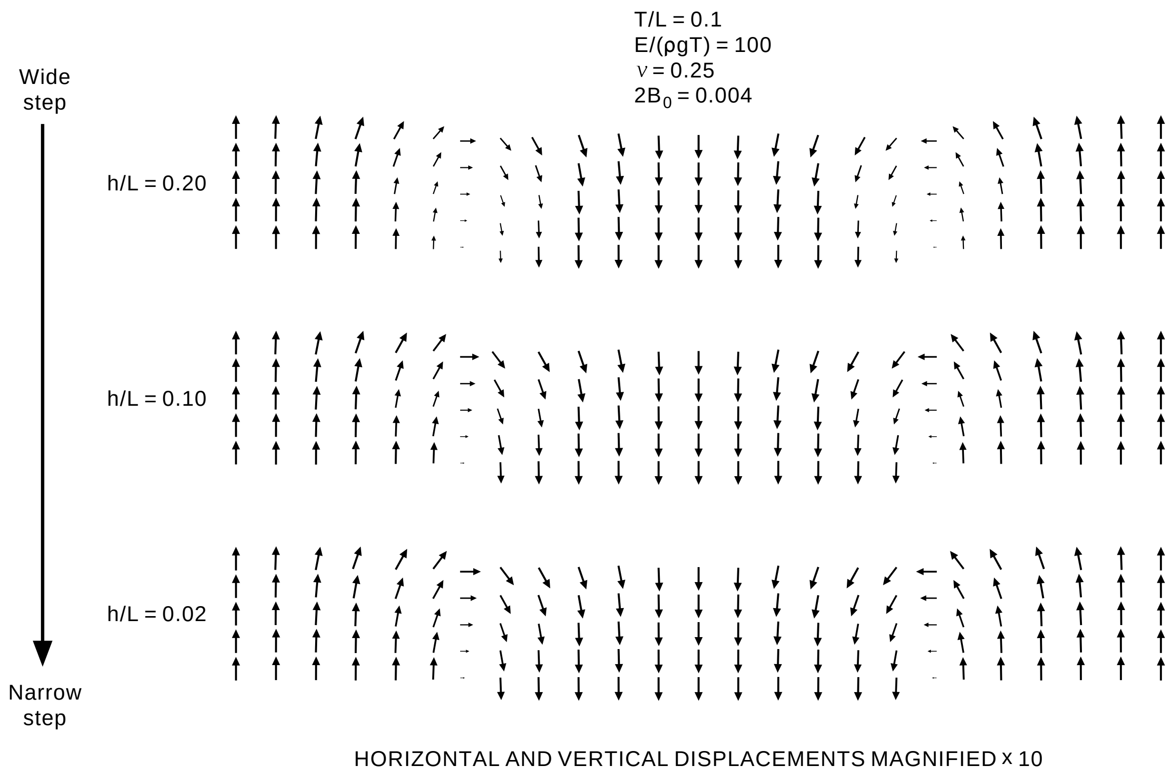

Figure 2. Displacement fields produced by draping of a single compressible elastic layer over a pair of facing steps. Variables are: T—layer thickness, L—fold wavelength, E—Young's modulus, g—gravitational acceleration, ν—Poisson's ratio, B—height of step, h—width of step. In order to examine the effects of changing step geometry, the ratio h/L is decreased from 0.20 in the uppermost layer to 0.02 in the lowermost layer, thereby concentrating displacement gradients (i.e., strains) above the steps. In order to emphasize the perturbed stress fields near the steps, gravitational body forces were not included in these calculations.

PWS-0196-0071

Bell and others (1992) describe a similar situation, in which fissures are located in the hanging walls of reactivated faults near Las Vegas, Nevada. An opening mode crack that starts at the Earth's surface, in contrast, can be expected to propagate downward only a short distance before compressive lithostatic stresses terminate fracture growth. One might therefore predict that fissures developed along downward propagating cracks will be relatively shallow and quickly filled with sediment, and that fissures developed along upward propagating cracks will be relatively deep and persistent (see Schumann, Morton, Ward and others, Carpenter, and Haneberg and Friesen abstracts for discussions of other earth fissures related to their development). This is not to say that all earth fissures must form along opening mode cracks that originate at depth, particularly because supporting field evidence is weak at best, but rather that the development of tension at depth may be one way to initiate the fissuring process.

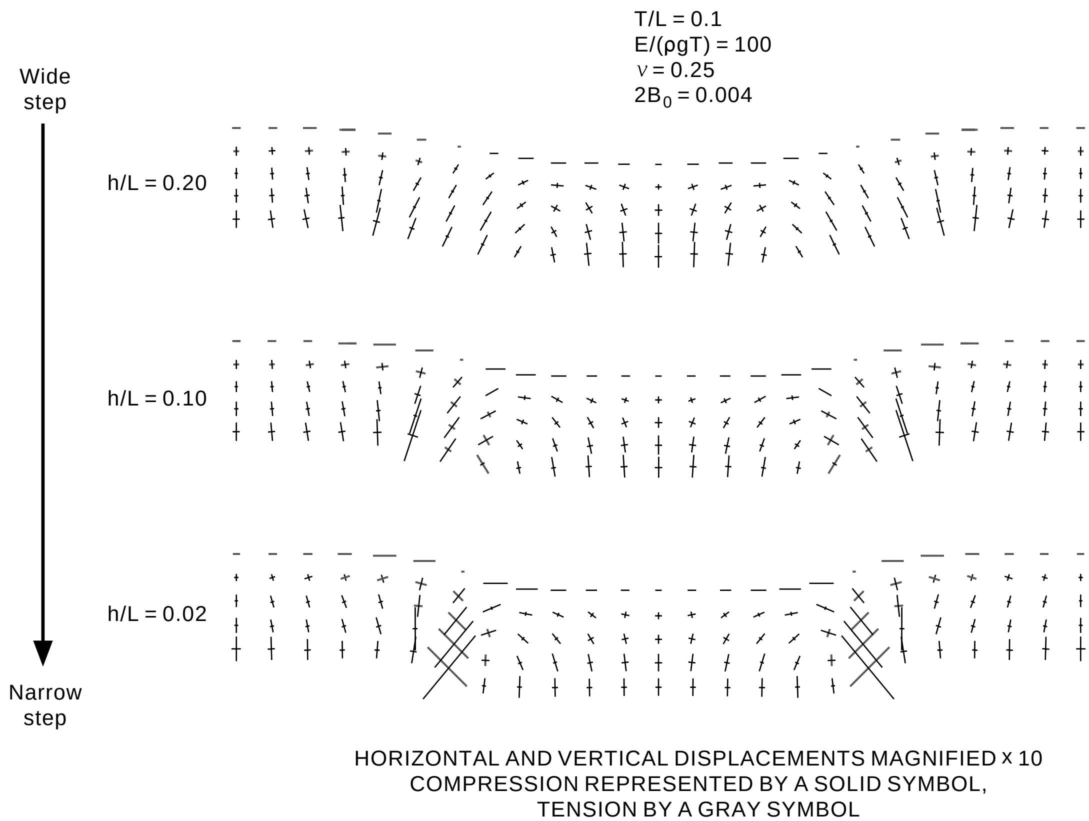

Figure 3. Principal stress fields produced by draping of a single compressible elastic layer over a pair of facing steps. Variables are identical to those in figure 2. The magnitude of principal stresses is proportional to length. Tensile stresses, which may initiate fissuring at depth in unconsolidated or poorly consolidated sedimentary aquifers, develop along the step as the ratio h/L is decreased. In order to emphasize the perturbed stress fields near the steps, gravitational body forces were not included in these calculations.

PWS-0196-0072

HYDRAULIC FORCES THAT PLAY A ROLE IN GENERATING FISSURES AT DEPTH

Donald C. Helm (U. S. Geological Survey, Carson City, Nevada, and
Nevada Bureau of Mines and Geology, Reno, Nevada)

Throughout the southwestern United States, fissures are observed to develop in sedimentary material in response to ground-water withdrawal. To explain and also to predict their occurrence, the principal driving force must be identified and quantified. The principal driving force on the aquifer (saturated assemblage of solid particles) is the difference between the driving force on the entire bulk material of solids and water together and the driving force on the water relative to the solids. The latter is the seepage force and is directly measurable as the gradient of hydraulic head. What is new in the present paper is a deeper understanding of the role played by the driving force on the bulk material.

In response to pumping an idealized confined aquifer at a constant rate Q, the net driving force on the skeletal frame turns out to be the gradient of excess pore-water pressure (Helm, 1994). The concept of excess pore-water pressure was introduced by soil engineers (Bjerrum, 1969) to represent the difference between the observed transient gradient of hydraulic head and the calculated ultimate steady-state gradient of hydraulic head.

More generally, the so-called steady-state gradient becomes the bulk driving force (Helm, 1994). It can be considered to be essentially a mathematical way to extend to interior points the physical effect of boundary flows (fig. 1) or pressure conditions that may themselves be steady or transient. Under many circumstances, such as pumping at a steady rate, the physically real driving force on bulk material reduces eventually to the familiar steady-state gradient of hydraulic head.

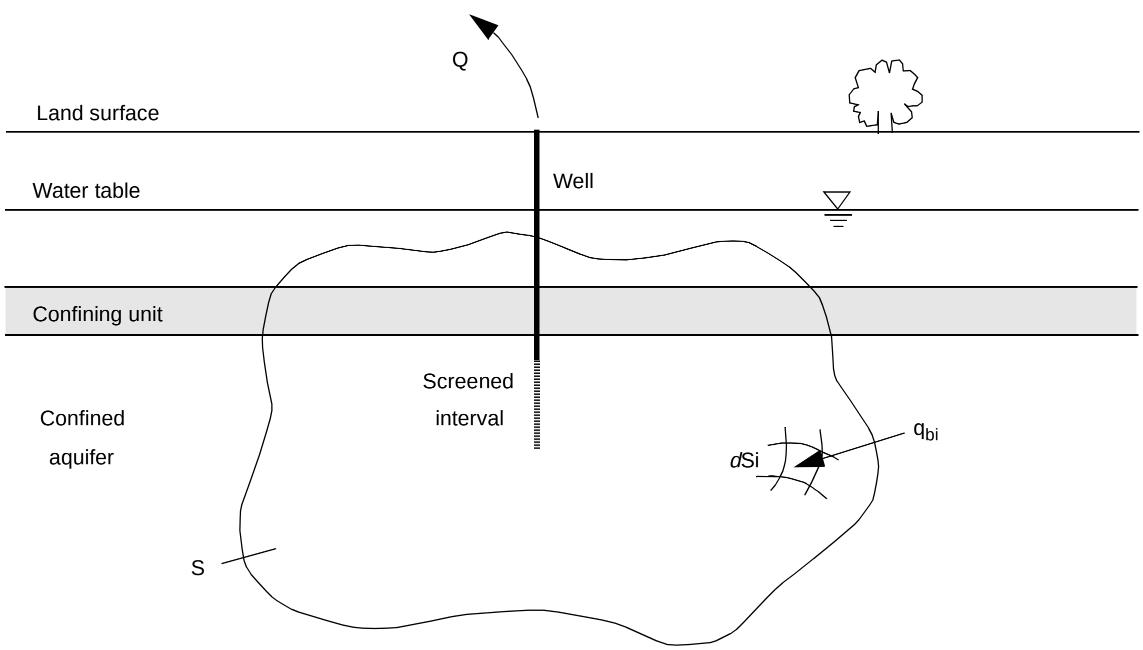

Figure 1. Concept of bulk flux around a pumping well.

PWS-0196-0073

The concept of bulk flux can be explained in the following way (see fig. 1). For any arbitrary closed surface S (fixed in space) that contains a sink (such as a screened interval) from which water is being withdrawn at a flow rate Q, if the constituent materials (such as the interstitial water and the grains and platelets that comprise the aquifer) are individually incompressible, then starting immediately upon turning on the pump a bulk flux q_b of solids and/or water must flow through S. This phenomenon is required by the conservation of mass. One can in fact write:

$$Q = \sum_{i=1}^{m} q_{bi} dS_i ,$$

where q_{bi} is the bulk flux moving through an incremented area dS_i and where m such incremented areas compose S. This flow is required through any closed surface within saturated sedimentary material for as long as Q is being withdrawn.

Another result of this analysis is that when a pump is turned on, the aquifer and water together are predicted to be set in motion as bulk flux towards the discharging well. This is a direct consequence of the principle of mass balance and the fact that if the expansion of individual solid grains (which comprise the skeletal assemblage) and the expansion of interstitial water alone are not sufficient to supply the entire flow rate Q from the well, then porosity near the well must decrease (fig. 2). The aquifer skeleton must move inward a sufficient distance and at a sufficient rate so that it remains contiguous. This net movement is also predicted to occur at distant points even where no change in porosity may have occurred locally. In fact, this movement can be quantified.

For the sake of illustration, assume that water and individual grains are much less compressible than the aquifer's skeletal structure (porosity). Ultimately (after long enough time), the flow rate Q is supplied by steady-state flow of incompressible water past a skeletal frame that has come to rest. Initially, however, Q is supplied by bulk flow as water and the skeletal frame (solids) flow together as undifferentiated incompressible material. In addition, water and solids move initially with the same velocity. As a direct consequence of mass conservation, the bulk material satisfies the equation of incompressible flow throughout time. A major change that occurs with time is that ultimately bulk flow consists entirely of water flowing past solids whereas initially there is no such relative flow. Hence, because there is initially no relative flow (namely, water flowing past solids), there is initially no seepage force. In other words, there is no gradient of observed hydraulic head initially even though the contiguous aquifer is indeed

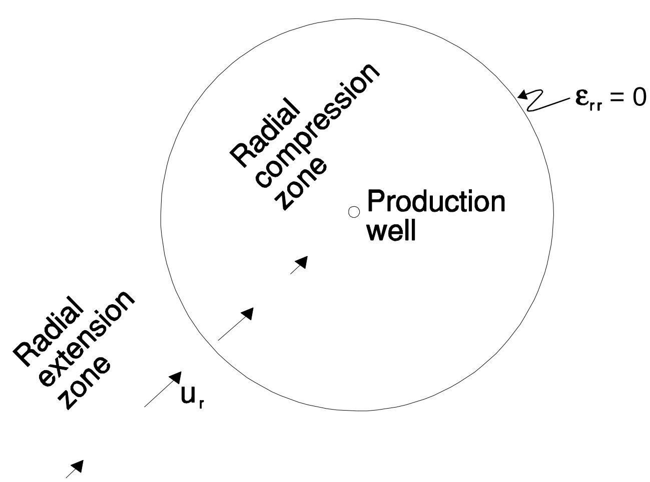

Figure 2. Inner zone of radial compression and surrounding outer zone of radial extension near a production well in a confined aquifer.

PWS-0196-0074

moving. During intermediate time, a transient zone of drawdown develops near the well and expands outward (fig. 2). This zone coincides with a zone of decrease in porosity and a zone of relative flow. This zone of drawdown does not, however, delineate the zone of bulk movement itself. To summarize: At any fixed point of interest, bulk movement in a Theis aquifer remains a constant in response to constant Q. It merely makes a gradual transition from flow of solids and water together to flow of water alone.

The process discussed above is illustrated for a confined aquifer in figure 2. The arrows in figure 2 represent the cumulative radial displacement u_r of the aquifer over a specified period of time Δt. Aquifer movement is everywhere inward towards the discharging well. If a front grain travels a shorter distance during Δt than a neighboring back grain travels, radial compression results. If the front grain travels a longer distance than the back grain, radial extension results. For radial compression, the radial strain ε_{rr} ($= \partial u_r/\partial r$) is positive; for extension, it is negative. Along the boundary between the two zones the radial strain ε_{rr} is zero and at this boundary, radial aquifer displacement has reached a maximum (see fig. 2). This boundary itself moves outward with time as the inner zone of aquifer compression gradually expands. Due to axial symmetry, tangential strain $\varepsilon_{\theta\theta}$ equals simply u_r/r and is everywhere compressive. Hence wherever radial extension equals $-u_r/r$ in the outer zone, the sum $\varepsilon_{rr} + \varepsilon_{\theta\theta}$ equals zero and correspondingly there is locally no change in horizontal porosity. Consequently, drawdown in this outer area is unlikely to occur even though the radially inward movement of the aquifer u_r is locally occurring. In fact, in this outermost area of figure 2, u_r can be calculated based directly on the mass balance discussion of figure 1.

The fact that turning on a pump immediately imparts an initial and radially inward velocity onto the skeletal frame has far-reaching consequences. According to Newton's first law, an external force is required to stop the ongoing inward motion of the skeletal frame. Such an external force can be supplied by the well screen itself. It can also be supplied by subvertical heterogeneities within the aquifer with more cohesive or massive material on the far side, for example by distant bedrock intersecting the aquifer at depth. The fundamental question is now reversed. To find how fissures are generated at depth, one must search for forces that impede aquifer movement after the pump is turned on rather than forces that drive it. The natural state of the aquifer is to be moving towards the discharge center—even at distant points where no drawdown is occurring.

Two competing mechanisms have been posited in the past to explain the generation of fissures. They can now be placed in perspective. One of the former explanations (Lofgren, 1978) is the viscous drag of flowing water on a solid particle (fig. 3) caused by horizontal seepage forces (gradients of hydraulic head). Such an explanation is sufficient for an isolated grain, but is incomplete for a radially extensive and contiguous assemblage of grains as has been discussed above. The role of the bulk hydraulic force, which imparts an initial velocity to all particles (namely, both slightly compressible or incompressible fluid particles and incompressible solid particles), has been traditionally overlooked.

The other posited explanation from the past (Lee and Shen, 1969; Jachens and Holzer, 1979) is the horizontal tension caused by flexure of a bending horizontal elastic beam or plate (fig. 4). Bending along the top is caused by an assumed vertical movement along the base of the beam or plate. The center of a subsidence bowl represents the greatest vertical movement beneath the plate, and the perimeter of the bowl represents the least vertical movement. This mechanism qualitatively explains the observed radial inward movement of the land surface.

The bending beam analogy predicts that fissures will occur along the shoulder of a subsidence bowl where horizontal extension is greatest. It also predicts that cracks will open first at the land surface and then propagate downwards. On the basis of on field observations, subsidence-related cracks are universally interpreted to migrate upwards from depth and to express themselves at land surface as a final step. They

PWS-0196-0075

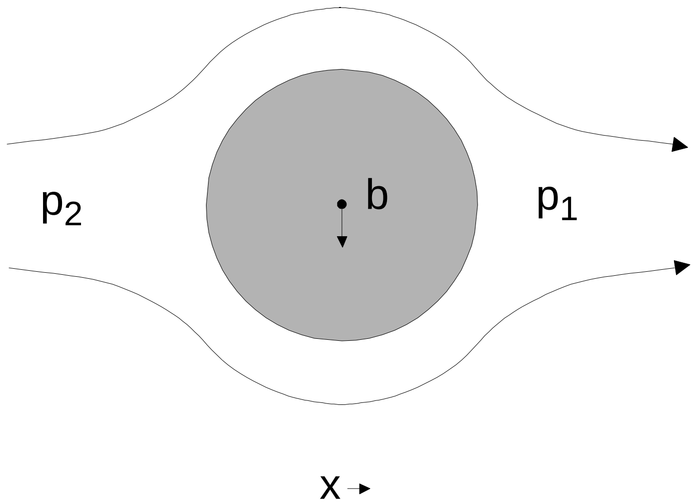

Figure 3. The seepage force analogy: Due to momentum balance, the forces acting on an isolated grain are (1) a submerged or buoyant body force b and (2) a surface force $(p_2-p_1)/(x_2-x_1)$ caused, in this case, by the viscous flow of water.

occur not only where predicted along the shoulders of a subsidence bowl where the curvature of vertical movement is convex upward but also beyond the outer perimeter of the subsidence bowl where essentially no subsidence nor drawdown has been observed. Fissures are also found near the center of a subsidence bowl where the curvature of vertical subsidence is concave upward (see Haneberg abstract for additional discussion on fissure migration).

In order to explain this last observation it may seem tempting at first glance to modify the original use of the bending beam analogy. If one considers the entire thickness of an actual bending beam, only the midplane has no horizontal component of movement. Originally, therefore, only the top half of the beam was considered appropriate to apply to the subsidence case. As mentioned above, this allows the base of the traditional bending beam to move vertically only. The modification is to consider the entire thickness. Because the bottom half of an entire bending beam is in extension where the top half is in compression, a tensional crack might conceivably originate at depth near the center of a subsidence bowl, pass through the neutral zone of the midplane and then somehow migrate upward to the land surface through the locally compressing upper half. Such a modification requires the horizontal component of aquifer movement at depth to be radially away from a discharging well. This radially outward motion at depth is opposite in direction from the hydraulic forces and opposite in direction from movement observed at land surface. To require the general horizontal direction of aquifer motion at depth to be away from a discharging well is fraught with insurmountable difficulties. One is left with the original upper-half bending elastic beam analogy (fig. 4) that has had essentially no predictive success.

The bending beam analogy should not be confused with the empirical draping effect. Draping describes the motion at land surface in response to differential vertical movement at depth caused, in turn, by heterogeneities or geologic structure (see Haneberg abstract for a more complete discussion of draping). For example, if gradual vertical slip occurs at depth across a buried subvertical fault due perhaps to different thicknesses of compressing clay on the two sides of the fault, one would expect a corresponding rotational movement at land surface with one side subsiding faster than the other. This would occur due to mass balance whether or not the bending beam analogy is applicable and whether or not elasticity is the appropriate constitutive relation for behavior of unconsolidated sedimentary material.

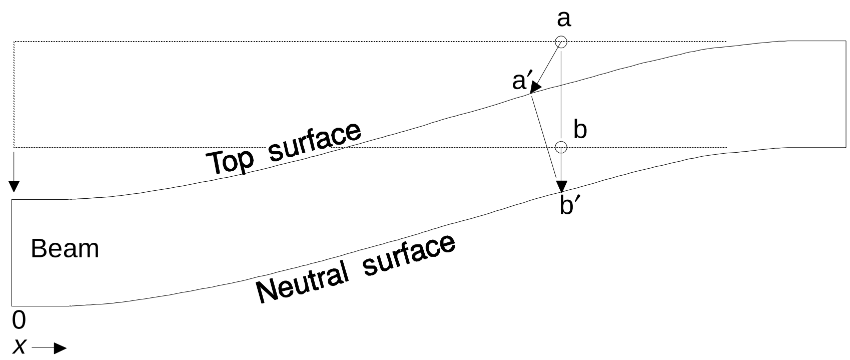

Figure 4. The bending beam analogy: point b on the neutral surface moves vertically downward to a new position b'. Point a, which lies above the neutral surface, rotates both downward and inward towards the point (x=0) where maximum vertical displacement occurs (analogous to the center of a subsidence bowl).

In conclusion, mass balance and Darcy's law for the flow of water relative to the solid matrix require that a porous nonrigid aquifer moves radially towards a discharging well. A bulk hydraulic force allows such movement to occur in outlying areas near the perimeter of a sedimentary basin even before drawdown occurs locally. For known boundary conditions and material properties, this movement can be predicted quantitatively for a continuum. Fissures are predicted to occur where geologic structure and heterogeneities impede this motion and more specifically where preexisting planes or points of weakness allow a crack to be generated.

PWS-0196-0077

SIMULATION OF THREE-DIMENSIONAL GRANULAR DISPLACEMENT IN UNCONSOLIDATED AQUIFERS

Thomas J. Burbey (U.S. Geological Survey, Carson City, Nevada)

Hydrodynamic processes associated with land subsidence and subsequent earth fissuring due to fluid withdrawal in unconsolidated aquifers are three dimensional in scope. Mathematical and numerical models that use hydraulic head or volume strain as the principal unknown variable are traditionally one dimensional with respect to changes in storage and strain. These models can simulate the total vertical compaction of interbeds in a confined aquifer, but they have no way of predicting directional components of granular movement or the resulting strain field. Consequently, they cannot estimate where damaging fissures may occur over time. For research purposes a new three-dimensional numerical model is being developed that is based on the modular finite-difference ground-water flow model (MODFLOW) by McDonald and Harbaugh (1988) that has the displacement field of solids as its principal unknown variable (see Leake abstract for the current status of MODFLOW and packages for simulating land subsidence). The governing equation (Helm, 1987) can be written as:

$$\frac{d}{dt}\vec{u} - \frac{\bar{K}}{\rho_w g \alpha}\nabla(\nabla \bullet \vec{u}) = \vec{q}_b - \vec{q}_o + \frac{\bar{K}}{\rho_w g}\nabla\sigma_m$$

where $\vec{u}$ is the displacement of solids, K is the hydraulic conductivity tensor, ρ_w is the density of water, g is the gravity constant, α is the compressibility of the skeletal matrix, $\vec{q}_b$ is the bulk flux, $\vec{q}_o$ is the initial unstrained specific discharge, and σ_m is the mean total stress. Because the displacement field of solids is a vector quantity, granular displacement resulting from imposed stresses on an unconsolidated aquifer can be simulated in three dimensions. The new model is not limited to confined aquifers, but can readily be applied to unconfined and semiconfined aquifers.

The three-dimensional governing equation used in the new model inherently assumes that ground-water flow is relative to solids. Thus, a new set of initial conditions is needed to account for the solid matrix. This quantity is the bulk flux that takes into account both the velocity of water and the velocity of solids (see Helm abstract). Expressions are developed for the bulk flux for both a pumping well (or artificial recharge well) and natural recharge by infiltration of precipitation.

The general three-dimensional form of the governing equation is difficult to apply numerically and does not comply to the general structure of the modular ground-water flow model. A more tractable and simpler approach is to uncouple the governing equation into three one- dimensional expressions. This was accomplished by assuming that within a specified material the changes or gradients of shear strain are small in comparison to the changes or gradients of normal strain in the principal directions. In this way the

PWS-0196-0078

displacement of solids can be viewed as a scalar quantity, much like hydraulic head in the ground-water flow equation. The result is a separate diffusion-style equation for each component direction as follows:

$$\frac{du_x}{dt} - \frac{K_{xx}}{3\rho_w g \alpha_{xx}}\left(\frac{\partial^2 u_x}{\partial x^2}\right) = q_{bx} - q_{ox} ,$$

$$\frac{du_y}{dt} - \frac{K_{yy}}{3\rho_w g \alpha_{yy}}\left(\frac{\partial^2 u_y}{\partial y^2}\right) = q_{by} - q_{oy} ,$$

$$\frac{du_z}{dt} - \frac{K_{zz}}{3\rho_w g \alpha_{zz}}\left(\frac{\partial^2 u_z}{\partial z^2}\right) = q_{bz} - q_{oz} ,$$

where the subscripts x, y, and z represent the principal directions. A Crank-Nicolson numerical procedure, which is second-order correct and unconditionally stable, is used to approximate the resulting three one-dimensional governing equations. The uncoupled expressions for each component direction form a tridiagonal matrix that can be solved directly. Boundary conditions are developed for both zero displacement and impermeable lateral boundaries. A zero volume-strain rate condition is used to simulate the location of the water table. The aquifer bottom, representing basement rock, is always assumed to be a zero-displacement boundary.

Hypothetical simulations are developed for unconfined isotropic, unconfined anisotropic, and confined isotropic aquifers. A 12-layered 1,000-ft-thick system with a single pumping well having a 100-ft-thick screened interval is used to test the new model. Simulation results for the isotropic condition indicate that displacement is symmetrical and inward toward the pumping well. The spherical radius of maximum inward displacement progresses outward from the well as simulation time increases. The shape of this “radius” becomes modified by boundary conditions such as the water table. Thus, for a short simulation time, the maximum downward vertical displacement is not at land surface but rather at a point nearer the screened interval of the pumping well. In fact, a poisson type of effect occurs as small upward displacements at the water table are simulated in a donut-shaped pattern around the well bore. For the anisotropic condition, when vertical hydraulic conductivity becomes small relative to horizontal hydraulic conductivity, the displacement field changes from mostly horizontal to mostly vertical. A dominant downward displacement is simulated in all layers above the screened interval for strongly anisotropic conditions (fig. 1A) The lateral extent at which a dominant downward component of displacement occurs depends on the degree of anisotropy. For the confined condition, displacement is primarily downward in the confining unit but is mostly horizontal within the homogeneous isotropic aquifer beneath the confining unit (fig. 1B). Near the well, vertical displacements become significant within the aquifer also. Within the region of horizontal compression in radially extensive confined aquifers, the displacement model simulates less vertical subsidence than conventional models that ignore horizontal granular movement.

.

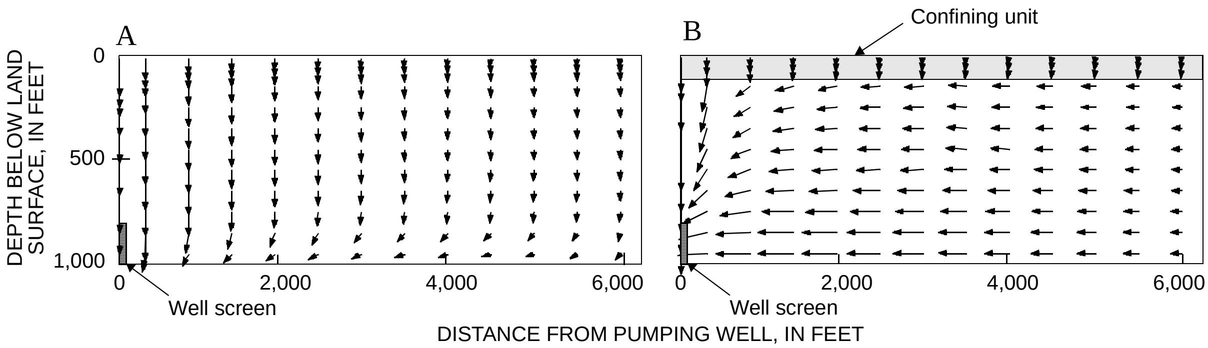

Aquifer Condition or Property	Anisotropic (fig. 1A)	Confined (fig. 1B)
Horizontal hydraulic conductivity of confining unit	not applicable	1.0 ft/day
Vertical hydraulic conductivity of confining unit	not applicable	0.0001 ft/day
Horizontal hydraulic conductivity of aquifer	10 ft/day	10 ft/day
Vertical hydraulic conductivity of aquifer	0.01 ft/day	10 ft/day
Elastic specific storage of confining unit	not applicable	2×10^{-5} $foot^{-1}$
Inelastic specific storage of confining unit	not applicable	8×10^{-4} $foot^{-1}$
Elastic specific storage of aquifer	2×10^{-6} $foot^{-1}$	2×10^{-6} $foot^{-1}$
Inelastic specific storage of aquifer	8×10^{-6} $foot^{-1}$	8×10^{-6} $foot^{-1}$
Maximum horizontal displacement	0.0073 foot	0.0261 foot
Maximum vertical displacement	0.3809 foot	0.0866 foot
Pumping rate	2.0 ft^3/s	2.0 ft^3/s
Total pumping time	500 days	500 days

Figure 1. Granular displacement in (A) an unconfined isotropic aquifer and in (B) a confined isotropic aquifer, with accompanying table describing values used for each simulation. Vector arrows indicate relative magnitude of displacement.

PWS-0196-0080

STATUS OF COMPUTER PROGRAMS FOR SIMULATING LAND SUBSIDENCE WITH THE MODULAR FINITE-DIFFERENCE GROUND-WATER FLOW MODEL

Stanley A. Leake (U.S. Geological Survey, Tucson, Arizona)

The Regional Aquifer-Systems Analysis (RASA) Program of the U.S. Geological Survey included studies of the Southwest Alluvial Basins in Arizona and New Mexico. Although land subsidence caused by ground-water pumpage occurs in this area, detailed analysis of land subsidence was beyond the scope of the Southwest Alluvial Basins RASA studies. Therefore, a follow-up RASA Subsidence-Modeling Study was initiated to develop improved methods of simulating aquifer-system compaction and land subsidence in models of ground-water flow. The purpose of this paper is to summarize the methods of simulating aquifer-system compaction that were developed by the Subsidence-Modeling Study.

The modular finite-difference ground-water flow model (MODFLOW) by McDonald and Harbaugh (1988) is widely used to simulate ground-water flow. MODFLOW was used for the Subsidence-Modeling Study because the modular structure of the computer program allows addition of new simulation capabilities in an organized way. In MODFLOW, simulation options are referred to as “packages.” The Subsidence-Modeling Study developed three packages for simulating aquifer-system compaction and land subsidence in MODFLOW. The first package is the Interbed-Storage Package, version 1, commonly referred to as IBS1. Similarly, the other two packages are referred to as IBS2 and IBS3. The name “Interbed Storage” refers to the ability of the packages to simulate storage changes and compaction in fine-grained interbeds within an aquifer; however, these packages also can be used to simulate compaction in extensive confining beds (for example, see Pool #1 abstract). All three packages are based on the theory of one-dimensional (vertical) consolidation developed by Terzaghi (1925). Each of the packages, however, uses a different set of simplifying assumptions and requires a different set of input arrays.

In the IBS1 package (Leake and Prudic, 1991), elastic and inelastic storage properties of compressible sediments are constant and head change is the stress that causes compaction. Delay in release of water from compressible interbeds is ignored. In the IBS2 package (Leake, 1990), storage properties also are constant and head change is the stress that causes compaction; however, IBS2 simulates the delay in release of water from compressible interbeds. For each model cell, IBS2 solves a one-dimensional equation to compute flow and compaction in an interbed of a representative or average thickness. Those results are extrapolated to compute compaction for the total thickness of interbeds in each cell. In the IBS3 package (Leake, 1991), compaction is computed as a function of effective stress, and elastic and inelastic specific storage can vary with changes in effective stress. The thickness of compressible sediments in an aquifer also can vary with changes in saturated thickness. The major assumptions for all three packages are outlined in table 1.

For confined aquifer systems in which geostatic load is constant and change in effective stress is small in relation to starting effective stress, use of the IBS1 package is appropriate. In some instances, the IBS1 package can be used in water-table aquifers by adjusting the elastic and inelastic storage coefficients to compensate for differences between magnitudes in change in head and change in effective stress. If an aquifer system includes thick interbeds for which delay in release of water cannot be ignored, the IBS2 package is the only package that can account for the delay. For unconfined aquifers or confined aquifers with varying geostatic load, the IBS3 package probably is the most appropriate. For comparison purposes, all three methods were applied to a model of ground-water flow in an alluvial basin in Arizona (Leake, 1992).

PWS-0196-0081

The amount of information needed to implement each package is related to the simplifying assumptions used for the package. The major arrays for all three packages are given in table 2. In addition to the arrays listed, all three packages read in a starting compaction array that allows continuation of a previous model run. Most of the information is read in as two-dimensional arrays for each model layer that includes compressible interbeds or a confining bed. The IBS1 package uses all four of the simplifying assumptions in table 1 but requires relatively few input arrays (table 2). Conversely, the IBS3 package uses only one of the assumptions in table 1 but requires many input arrays. In addition to the input arrays, IBS3 requires two additional arrays to store geostatic load and effective stress for which starting values are computed from input arrays.

Table 2. Assumptions for Interbed-Storage Packages IBS1, IBS2, and IBS3

	Assumption	IBS1	IBS2	IBS3
1.	A unit decrease in water level results in a unit increase in effective stress	✔	✔	
2.	A head change in coarse-grained aquifer materials in a model time step results in an equal head change in compressible interbeds	✔		✔
3.	Elastic and inelastic skeletal specific storages of compressible interbeds are constants	✔	✔	
4.	Total thickness of compressible interbeds is not a function of saturated thickness of the aquifer	✔	✔	

Table 3. Input arrays required for Interbed-Storage Packages IBS1, IBS2, and IBS3

Property or condition	Interbed-Storage Package		
	IBS1	IBS2	IBS3
Storage	1. Elastic storage coefficient 2. Inelastic storage coefficient	1. Elastic specific storage 2. Inelastic specific storage	1. Starting elastic specific storage 2. Starting inelastic specific storage
Hydraulic		3. Vertical hydraulic conductivity of interbeds	
Other	3. Starting preconsolidation head	4. Starting preconsolidation head 5. Starting head 6. Average interbed thickness 7. Number of interbeds	3. Starting preconsolidation stress 4. Elevation of land surface 5. Specific gravity of moist sediments 6. Specific gravity of saturated sediments 7. Void ratio 8. Starting total thickness of interbeds

PWS-0196-0082

The IBS1 package is formally documented for use inside and outside the U.S. Geological Survey (Leake and Prudic, 1991). The IBS2 and IBS3 packages were developed to study alternative methods of simulating land subsidence in ground-water flow models. The theoretical basis and mathematical development for these two packages are documented in Leake (1990) and Leake (1991); however, the computer programs are not formally documented. If either of these packages are needed for future land-subsidence studies, additional effort will be required to document the package prior to publication of the study results.

THE FREQUENCY DEPENDENCE OF AQUIFER-SYSTEM ELASTIC STORAGE COEFFICIENTS: IMPLICATIONS FOR ESTIMATES OF AQUIFER HYDRAULIC PROPERTIES AND AQUIFER-SYSTEM COMPACTION

Devin L. Galloway (U.S. Geological Survey, Sacramento, California)

Aquifer-system compaction resulting from reduced fluid pressures in interbedded alluvial aquifers is governed by the skeletal elastic storage coefficients of the aquifer, S_{ke}, and the interbeds, S'_{ke}, and the inelastic storage coefficient of the aquifer system, S^*_{kv}. The elastic skeletal components are related by:

$$S^*_{ke} = S_{ke} + S'_{ke},$$

where S^*_{ke} is the skeletal elastic storage coefficient of the aquifer system. Where measurements of aquifer-system compaction and aquifer fluid pressures are available, stress-strain diagrams (for example, see Carpenter abstract where stress-displacement diagrams are presented for horizontal movement across an earth fissure in the Picacho Basin, Arizona) can be computed and estimates of S^*_{ke} and S^*_{kv} can be obtained (Riley, 1969). Typically, this stress-strain relation is developed from the seasonal drawdown and recovery cycle associated with agricultural and municipal/industrial ground-water use. As such, the aquifer system storage estimates are representative of long period, low frequency responses of the aquifer system to stresses. Estimates of S'_{ke} are computed from S^*_{ke} and S_{ke}, where by contrast, estimates of S_{ke} are often obtained on the basis of short duration, high frequency responses of aquifer fluid pressures measured in wells to imposed hydraulic stresses, such as a pumping test or slug test. This approach for computing S'_{ke} may not be valid if the aquifer-system response to stress is dependent on the frequency of the imposed stress (Helm, 1974). The discussion that follows addresses only the elastic range of aquifer-system compaction.

For uncemented granular material the barometric efficiency of a well/aquifer system is inversely proportional to S, the aquifer storage coefficient (Jacob, 1940), and so the frequency response of barometric efficiency to atmospheric loading can serve to illustrate the relation between the elastic properties of the aquifer and the frequency of the applied load (fig. 1). The theoretical response (Quilty and Roeloffs, 1991) is computed for a 150-m-thick, partially confined aquifer, hydraulically connected to a water table 50 m below land surface through a specified vertical hydraulic diffusivity, D_v. For values of D_v typical of interbedded alluvial aquifer systems, between 1.0 x 10^2 and 1.0 x 10^4 m^2/d, the response is frequency dependent for frequencies less than about 0.1 and 10 cycles per day, respectively. The frequency-dependent part of these curves represents the influence of fluid flow and drainage of the aquifer system in response to a change in the atmospheric load. For small values of D_v, 1.0 m^2/d, characteristic of a confining unit, the response is frequency-independent for stress frequencies greater than 0.001 cycles per day. The frequency-independent part of these curves is known as the static-confined response and represents the mechanical, undrained response of the aquifer to loading.

This general relation between the decrease in barometric efficiency for lower frequencies of the applied load suggests that estimates of S^*_{ke} based on the cyclic annual recovery limb of a stress-strain diagram, with a frequency of 2.74 x 10^{-3} cycles per day (1 cycle/year), would be overestimated with regard to the aquifer-system confined response for a wide range of D_v. When used with estimates of S_{ke} derived from aquifer tests typically conducted at higher frequencies (over a period of hours to days), and more likely representative of the undrained aquifer-system confined response, the resultant estimates of S'_{ke} would also be overestimated. This approach for computing S'_{ke} leads to overestimation of the magnitude of aquifer-system rebound during the recovery cycle.

PWS-0196-0084

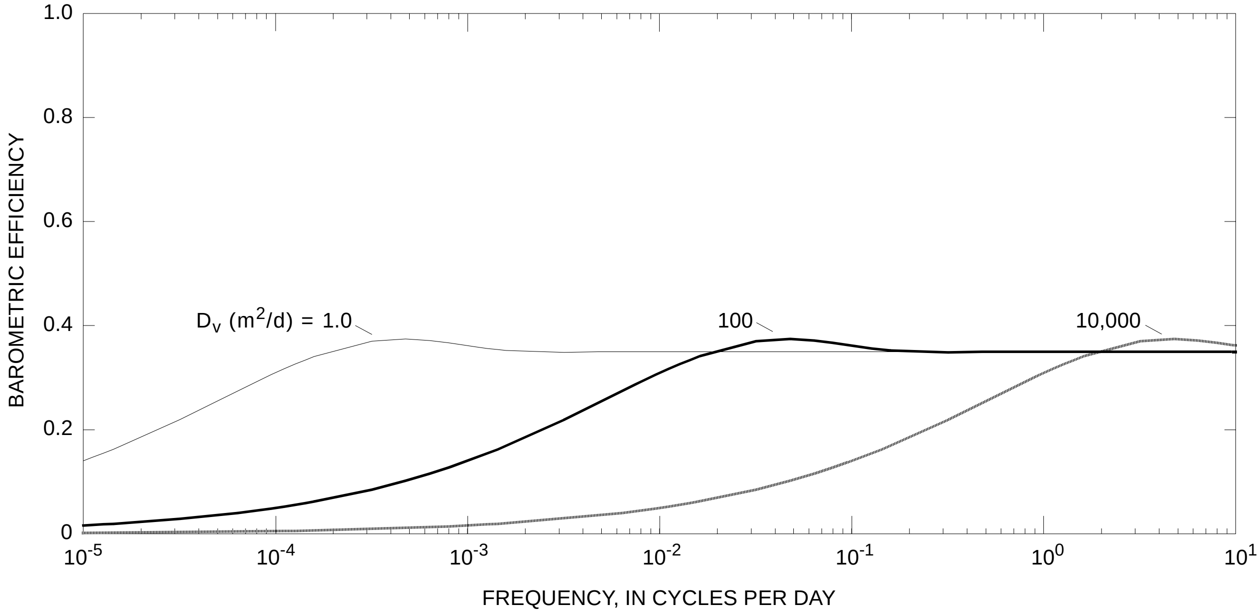

Figure 1. Theoretical response of the barometric efficiency of a well /aquifer to atmospheric loading. Barometric efficiency is plotted as a function of the frequency of the applied load, and the vertical hydraulic diffusivity, D_v. The static-confined barometric efficiency is 0.35.

Measurement and analytical techniques can be employed to compute the well/aquifer system frequency response to atmospheric loading (Rojstaczer, 1988; Quilty and Roeloffs, 1991), although information at frequencies less than about 0.05 cycles per day is difficult to obtain due to instrument drift and the required length of the barometric pressure and aquifer fluid pressure time series. Characteristics of the frequency response can be determined for higher frequencies that may reveal a frequency-dependent response from which estimates of D_v can be determined on the basis of the best fit to the theoretical response. If earth tides can also be measured, estimates of aquifer elastic skeletal specific storage, Ss_{ke}, and porosity, Φ, may also be computed (Bredehoeft, 1967; Rojstaczer and Agnew, 1989), where

$$Ss_{ke} = S_{ke}/b,$$

and b is the thickness of the aquifer. For these reasons it is useful to evaluate the potential for measuring barometric efficiency and the aquifer-system response to earth tides in alluvial aquifers with aquifer-system compaction.

The relation between Ss_{ke} and barometric efficiency (fig. 2) and Ss_{ke} and the tidal areal strain sensitivity (fig. 3) can be determined when *a priori* estimates of Poisson's ratio, ν, and the solid grain compressibility of the aquifer, β_s, are known or can be estimated (Rojstaczer and Agnew, 1989). The areal strain sensitivity is the ratio of the aquifer fluid-pressure response measured as the open water-level fluctuation in a well to the imposed areal strain of the solid earth tide in parts per million. For the range of Ss_{ke}, 1.0 x 10^{-6} to 1.0 x 10^{-5} m^{-1}, representative of alluvial aquifers where aquifer-system compaction has been measured (Ireland and others, 1984; Hanson, 1989), the barometric efficiency and the areal strain sensitivity are strongly dependent on Φ, especially near the lower end of the range. Larger barometric efficiencies occur with relatively small values of Ss_{ke}, and large values of Φ. Larger areal strain sensitivities similarly occur with relatively small values of Ss_{ke}, but unlike for atmospheric loading, small values of Φ. For midrange values of Ss_{ke} and Φ, barometric efficiencies between 0.1 and 0.5, and areal strain sensitivities between 0.2 and 0.5 m/microstrain could be expected.

PWS-0196-0085

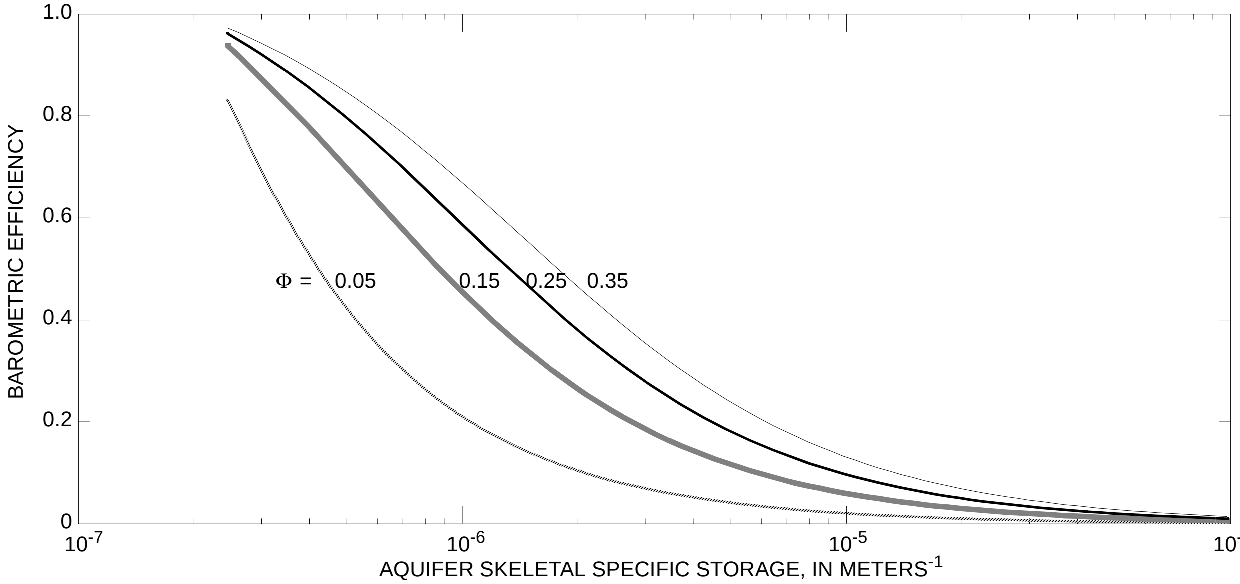

Figure 2. Barometric efficiency of a well/aquifer under static-confined conditions as a function of the aquifer skeletal specific storage, Ss_{ke}, and aquifer porosity, Φ. The compressibility of the solid grains, β_s, is 2.0×10^{-11} Pa^{-1} and Poisson's ratio, ν, is 0.25.

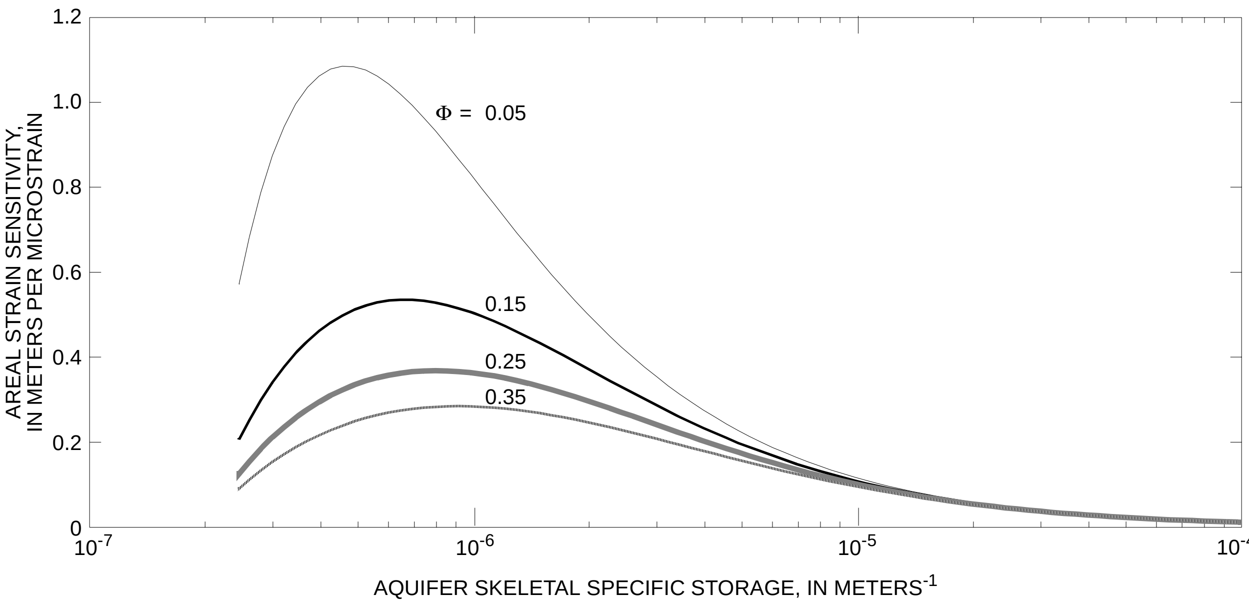

Figure 3. Sensitivity of an aquifer to areal strain under static-confined conditions as a function of the aquifer skeletal specific storage, Ss_{ke}, and aquifer porosity, Φ. The compressibility of the solid grains, β_s, is 2.0×10^{-11} Pa^{-1} and Poisson's ratio, ν, is 0.25.

Diurnal and semidiurnal fluctuations in barometric pressure at land surface typically comprise the smallest cyclical changes in barometric pressure and occur in the range of 0.02 to 0.03 m (equivalent height of water). A well with a static-confined barometric efficiency of 0.1 would produce a static-confined water-level fluctuation of about 0.002 to 0.003 m. A well with a static-confined areal strain sensitivity of 0.2 m/microstrain, responding to an areal strain of 0.012 microstrain (typical of the O_1 tide,

PWS-0196-0086

the smaller of the two principal lunar tides), would produce a static-confined water-level change of about 0.0024 m. These conservative estimates of the well responses represent measurable water-level fluctuations attainable with widely available submersible pressure transducers and recording data loggers capable of resolving 0.00075 m of water-level change.

Within the range of expected hydraulic properties of alluvial aquifers where compaction is occurring, it is likely that the frequency response of an aquifer system to atmospheric loading and the sensitivity of the areal strain of an aquifer to earth tides can be determined. These responses can provide insight into the frequency dependence of the skeletal elastic storage coefficients, as well as provide estimates of aquifer hydraulic properties including Ss_{ke}, Φ, and D_v.

PWS-0196-0087

ACKNOWLEDGMENTS

The U.S. Geological Survey Subsidence Interest Group gratefully acknowledges the support of Edwards Air Force Base and the National Aeronautical and Space Administration, Ames-Dryden Research Facility for hosting the conference. We are especially grateful to Mr. Larry Plews, Air Force Flight Test Center, for coordinating our use of the facilities, and for participating in the conference representing Edwards Air Force Base. Mr. Mel Marmet, Air Field Manager, provided access to Rogers Lake and facilitated our field trip. Finally, we are grateful to all those who attended the conference, those who prepared and made oral presentations, and those who submitted abstracts for this publication.

REFERENCES CITED

Beck, B.F., and Sayed, Sayed, 1991, The sinkhole hazard in Pinellas County—A geologic summary for planning purposes: Orlando, Florida Sinkhole Research Institute Report 90-91-1, 58 p.

Beck, B.F., and Sinclair, W.C., 1986 Sinkholes in Florida—An introduction: Orlando, Florida Sinkhole Research Institute Report 85-86-4, 18 p.

Bell, J.W., Price, J.G., and Mifflin, M.D., 1992, Subsidence-induced fissuring along preexisting faults in Las Vegas Valley, Nevada, *in* Stout, M.L., ed., Proceedings of 35th Annual Meeting of the Association of Engineering Geologists, October 2–9, 1992, Long Beach, California, p. 66–75.

Bjerrum, L., 1969, Soil with water—transient flow, *in* Lambe, T.W., and Whitman, R.V., eds., Soil Mechanics: New York, John Wiley and Sons, p. 388–522.

Blodgett, J.C., and Williams, J.S., 1992, Land subsidence and problems affecting land use at Edwards Air Force Base, California, 1990: U.S. Geological Survey Water-Resources Investigations Report 92-4035, 25 p.

Bredehoeft, J.D., 1967, Response of well-aquifer systems to earth tides: Journal of Geophysical Research, v. 72, p. 3075-3087.

California State Water Resources Control Board, 1974, Water quality control plan report, South Lahontan basin: California State Water Resources Control Board, 300 p.

Carpenter, M.C., 1993, Earth-fissure movements associated with fluctuations in ground-water levels near the Picacho Mountains, south-central Arizona, 1980–84: U.S. Geological Survey Professional Paper 497-H, 116 p.

Collins, James, 1989, Fundamentals of GPS baseline and height determinations: American Society of Civil Engineers, Journal of Surveying Engineering, v. 115, no. 2, p. 223–235.

Contaldo, G.J., and Mueller, J.E., 1991, Earth fissures of the Mimbres Basin, southwestern New Mexico: New Mexico Geology, v. 13, p. 69–74.

Dibblee, T. W., Jr., 1967, Areal geology of the western Mojave Desert, California: U.S. Geological Survey Professional Paper 522, 153 p.

Dixon, G.L., and Ward, A.W., 1994a, Preliminary geologic map of the Edwards Quadrangle, Kern County, California: U.S. Geological Survey open-file map, map scale 1:24,000.

Dixon, G.L., and Ward, A.W., 1994b, Preliminary geologic map of the Rogers Lake South Quadrangle, Los Angeles and Kern Counties, California: U.S. Geological Survey open-file map, map scale 1:24,000.

Dixon, T.H., 1991, An introduction to the Global Positioning System and some geological applications: Reviews of Geophysics, v. 29, no. 2, p. 249–276.

Durbin, T.J., 1978, Calibration of a mathematical model of the Antelope Valley ground-water basin, California: U.S. Geological Survey Water-Supply Paper 2046, 51 p.

Epstein, V.J., 1987, Hydrologic and geologic factors affecting land subsidence near Eloy, Arizona: U.S. Geological Survey Water-Resources Investigations Report 87-4143, 28 p.

Federal Geodetic Control Committee, 1989, Geometric geodetic accuracy standards and specifications for using GPS relative positioning techniques, Version 5.0 with corrections: National Geodetic Survey, National Oceanic and Atmospheric Administration, 48 p.

Fernandez, Gabriel, 1991, Report of brine field subsidence, Appendix B, *in* Haley and Aldrich of New York. A projection of future geologic conditions in the Tully Valley, Onondaga County, New York: Rochester, New York, v. 2, appendices, 17 p.

Fett, J.D., 1968, Geophysical investigation of the San Jacinto Valley, Riverside County, California: Riverside, California, University of California, M.A. thesis, 87 p.

Fett, J.D., Hamilton, D.H., and Fleming, F.A., 1967, Continuing surface displacement along the Casa Loma and San Jacinto faults in San Jacinto Valley, Riverside County, California: Engineering Geology, v. 4, p. 22–32.

Friesen, R.L., 1992, Cyclic flexure of surficial strata near an earth fissure in the Mimbres Basin, southern New Mexico: Socorro, New Mexico Institute of Mining and Technology, M.S. thesis, 86 p.

Getchell, F. A., 1982, Subsidence in the Tully Valley, New York: Syracuse University, unpublished master of science thesis, 144 p.

Haneberg, W.C., 1992, Drape folding of compressible elastic layers, I. Analytical solutions for vertical uplift: Journal of Structural Geology, v. 14, no. 6, p. 713-721.

Haneberg, W.C., 1993, Drape folding of compressible elastic layers, II. Matrix solution for two-layer folds: Journal of Structural Geology, v. 15, in press.

Haneberg, W.C., and Friesen, R.L., 1993, Tilting of surficial strata and groundwater level fluctuations in the subsiding Mimbres Basin, New Mexico: Las Cruces, New Mexico Water Resources Research Institute Report 274, 85 p.

Haneberg, W.C., Reynolds, C.B., and Reynolds, I.B., 1991, Geophysical characterization of soil deformation associated with earth fissures near San Marcial and Deming, New Mexico, *in* Johnson, A.I., ed., Land Subsidence—Proceedings of Fourth International Symposium on Land Subsidence, Houston, Texas, May 12–18, 1991: International Association of Hydrological Sciences Publication no. 200, p. 271–280.

Hanson, R.T., 1989, Aquifer system compaction, Tucson Basin and Avra Valley, Arizona, U.S. Geological Survey Water-Resources Investigations Report 88-4172, 69 p.

Helm, D.C., 1974, Evaluation of stress-dependent aquitard parameters by simulating observed compaction from known stress history: Berkeley, University of California, Ph.D. dissertation, 175 p.

Helm, D.C., 1987, Three-dimensional consolidation theory in terms of the velocity of solids: Geotechnique, v. 37, no. 3, p. 369–392.

Helm, D.C., 1992, Forces that play a role in generating fissures at depth, *in* Stout, M.L., ed., Proceedings of 35th Annual Meeting of the Association of Engineering Geologists, October 2–9, 1992: Long Beach, California, p 7-16.

Helm, D.C., 1994, Horizontal aquifer movement of a Theis-Thiem confined system: Water Resources Research, v. 30, no. 4, p. 953–964.

Holzer, T.L., 1981, Preconsolidation stress of aquifer systems in areas of induced land-subsidence: Water Resources Research, v. 1, no. 3, p. 693–704.

Holzer, T.L., ed., 1984, Man-induced land subsidence: Reviews in Engineering Geology, v. 6, 221 p.

Holzer, T.L., Davis, S.N., and Lofgren, B.E., 1979, Faulting caused by groundwater extraction in south-central Arizona: Journal of Geophysical Research, v. 84, no. B2, p. 603–612.

Ikehara, M.E., and Phillips, S.P., 1994, Determination of land subsidence related to ground-water-level declines using global positioning system and leveling surveys in Antelope Valley, Los Angeles and Kern Counties, California, 1992, U.S. Geological Survey Water-Resources Investigations Report 94-4184, 101 p.

Ireland, R.L., Poland, J.F., and Riley, F.S., 1984, Land subsidence in the San Joaquin Valley, California, as of 1980: U.S. Geological Survey Professional Paper 437-I, 93 p.

Jachens, R.C. and Holzer, T.L., 1979, Geophysical investigations of ground failure related to ground-water withdrawal—Picacho Basin, Arizona: Ground Water, v. 17, p. 574–585.

Jacob, C.E., 1940, The flow of water in an elastic artesian aquifer: EOS, American Geophysical Union Transactions, v. 21, p. 574–586.

Land, L.F., and Armstrong, C.A., 1985, A preliminary assessment of land-surface subsidence in the El Paso area, Texas: U.S. Geological Survey Water- Resources Investigations Report 85-4155, 96 p.

Langbein, J., Hill, D.P., Parker, T.N., and Wilkinson, S.K., 1993, An episode of reinflation of the Long Valley caldera, eastern California, 1989–1991: Journal of Geophysical Research, v. 98, p. 851–870.

Langbein, J.O., Hill, D.P., Parker, T.N., Wilkinson, S.K., and Pitt, A.M., 1990, Renewed inflation of the resurgent dome in Long Valley caldera, California, from mid-1989 to mid-1990 (abstract): EOS, American Geophysical Union Transactions, v. 71, no. 43, p. 1466.

Larsen, M.K., and Péwé, T.L., 1986, Origin of land subsidence and earth fissuring, northeast Phoenix, Arizona: Bulletin of the Association of Engineering Geologists, v. 23, p. 139–161.

Leake, S.A., 1990, Interbed storage changes and compaction in models of regional ground-water flow: Water Resources Research, v. 26, no. 9, p. 1939–1950.

PWS-0196-0089

Leake, S.A., 1991, Simulation of vertical compaction in models of regional ground-water flow, in Johnson, A.I., ed., Land subsidence—Proceedings of Fourth International Symposium on Land Subsidence, Houston, Texas, May 12–18, 1991: International Association of Hydrological Sciences Publication no. 200, p. 565–574.

Leake, S.A., 1992, Computer simulation of land subsidence from groundwater withdrawal in unconfined aquifers: Seismological Press, Proceedings of International Workshop on Groundwater and Environment, Beijing, China, August 16–18, 1992, p. 286–292.

Leake, S.A., and Prudic, D.E., 1991, Documentation of a computer program to simulate aquifer-system compaction using the modular finite-difference ground-water flow model: U.S. Geological Survey Techniques of Water-Resources Investigations, Book 6, Chapter A2, 68 p.

Lee, K.L., and Shen, C.K., 1969, Horizontal movements related to subsidence: Journal of the Soil Mechanics and Foundation Division, American Society of Civil Engineers, v. 95, no. SM1, p. 139-166.

Lewis, R.E., and Miller, R.E., 1968, Geologic and hydrologic maps of the southern part of Antelope Valley, California, supplement to U.S. Soil Conservation Service Report on the cooperative soil survey of Antelope Valley area, California: U.S. Department of Agriculture Report, 13 p.

Lofgren, B.E., 1976, Land subsidence and aquifer-system compaction in the San Jacinto Valley, California: Journal of Research of the U.S. Geological Survey, v. 4, no. 1, p. 9–18.

Lofgren, B.E., 1978, Hydraulic stresses cause ground movement and fissures, Picacho, Arizona?: Geological Society of America Abstract with Programs, v. 10, no. 3, p. 271.

Lofgren, B.E., and Rubin, Meyer, 1975, Radiocarbon dates indicate rates of graben downfaulting, San Jacinto Valley, California: Journal of Research of the U.S. Geological Survey, v. 3, no. 1, p. 45–46.

Londquist, C.J., Rewis, D.L., Galloway, D.L., and McCaffrey, W.J., 1993, Hydrogeology and land subsidence, Edwards Air Force Base, Antelope Valley, California: U.S. Geological Survey Water-Resources Investigations Report 93-4114, 74 p.

Mabey, D. R., 1960, Gravity survey of the western Mojave Desert, California: U.S. Geological Survey Professional Paper 316-D, p. 51–73.

McDonald, M.G., and Harbaugh, A.W., 1988, A modular three-dimensional finite-difference ground-water flow model: U.S. Geological Survey Techniques of Water-Resources Investigations, Book 6, Chapter A1, 548 p.

Milbert, D.G., 1991a, Computing GPS-derived orthometric heights with the GEOID90 geoid height model: ACSM-ASPRS Fall Convention, Atlanta, Georgia, October 28–November 1, 1991, p. A46–55.

Milbert, D.G., 1991b, GEOID90—A high-resolution geoid for the United States: EOS, v. 72, no. 49, p. 545.

Morin, R.L., Mariano, John, and Jachens, R.C., 1990, Isostatic residual gravity map of Edwards Air Force Base and vicinity, Kern, Los Angeles, and San Bernardino Counties, California, U.S. Geological Survey Open-File Report 90-664, scale 1:62,500.

Morton, D.M., 1972, Geology of the Lakeview and Perris (7.5') quadrangles, Riverside County, California: California Division of Mines and Geology Map Sheet 19.

Morton, D.M., 1977, Surface deformation in part of the San Jacinto Valley, southern California: Journal of Research of the U.S. Geological Survey, v. 5, no. 1, p. 117–124.

Morton, D.M., and Sadler, P.S., 1989, Landslides flanking the northeastern Peninsular Ranges and in the San Gorgonio Pass area of southern California, *in* Sadler, P.M., and Morton, D.M., eds., Landslides in a semi-arid environment: Inland Geological Society Publication, v. 2, p. 183–197.

National Oceanic and Atmospheric Administration, Federal Geodetic Control Committee, 1980, Classification, standards of accuracy, and general specifications of geodetic control surveys: U.S. Department of Commerce, 12 p.

National Research Council, 1991, Mitigating losses from land subsidence in the United States: Report of the Committee on Ground Failure Hazards and Mitigation Research, Division of Natural Hazard Mitigation, Commission on Engineering and Technical Systems, National Academy Press, Washington, D.C., 58 p.

Neal, J.T., 1965, Geology, mineralogy, and hydrology of U.S. playas: Air Force Cambridge Research Laboratories, 176 p.

Okada, Y., 1985, Surface deformation due to shear and tensile faults in a half-space: Bulletin of the Seismological Society of America, v. 75, no. 4, p. 1135-1154.

Poland, J.F., editor, 1984, Guidebook to studies of land subsidence due to ground-water withdrawal: United Nations Educational, Scientific, and Cultural Organization, no. 40 of UNESCO Studies and Reports in Hydrology, Paris, France, 305 p.

Poland, J.F., Lofgren, B.E., Ireland, R.L., and Pugh, R.G., 1975, Land subsidence in the San Joaquin Valley as of 1972: U.S. Geological Survey Professional Paper 437-H, 78 p.

Proctor, R.J., 1962, Geologic features of a section across the Casa Loma fault, exposed in an aqueduct trench near San Jacinto, California: Geological Society of America Bulletin, v. 73, p. 1293–1296.

Quilty, E.G., and Roeloffs, E.A., 1991, Removal of barometric pressure response from water-level data, Journal of Geophysical Research, v. 96, no. B6, p. 10209–10218.

Riley, F.S., 1969, Analysis of borehole extensometer data from central California, in Tison, L.J., ed., Land Subsidence: Tokyo, International Association of Scientific Hydrology Publication 89, v. 2, p. 423–431.

Rojstaczer, S.A., 1988, Determination of fluid flow properties from the response of water wells to atmospheric loading: Water Resources Research, v. 24, p. 1927–1938.

Rojstaczer, S.A., and Agnew, D.C., 1989, The influence of formation material properties on the response of water levels in wells to earth tides and atmospheric loading: Journal of Geophysical Research, v. 94, no. B6, p. 12403–12411.

Savage, J.C., 1988, Principal component analysis of geodetically measured deformation in Long Valley caldera, eastern California: Journal of Geophysical Research, v. 93, no. B11, p. 13297–13305.

Sinclair, W.C., 1982, Sinkhole development resulting from ground-water withdrawal in the Tampa area, Florida: U.S. Geological Survey Water-Resources Investigations Report 81-50, 19 p.

Snyder, J.H., 1955, Ground water in California—The experience of Antelope Valley: Berkeley, University of California, Division of Agriculture Science, Giannini Foundation Ground-Water Studies No. 2, 171 p.

Templin, W.E., Phillips, S.P., Cherry, D.E., DeBortoli, M.L., and others, 1994, Land use and water use in the Antelope Valley, California, U.S. Geological Survey Water-Resources Investigations Report 94-4208, 97 p.

Terzaghi, Karl, 1925, Erdbaumechanik auf Bodenphysikalischer Grundlage: Wein Leipzig, Deuticke, 399 p.

Ventura County Board of Supervisors, 1988, Ventura County general plan, goals, policies, and programs—hazards appendix: Ventura County Board of Supervisors document No. 1D297-1.90 and No. I198, adopted May 24, 1988, 146 p.

Ward, A.W., and Dixon, G.L., 1994a, Preliminary geologic map of the Redman Quadrangle, Los Angeles and Kern Counties, California, U.S. Geological Survey open-file map; map scale 1:24,000.

Ward, A.W., and Dixon, G.L., 1994b, Preliminary geologic map of the Rogers Lake North Quadrangle, Kern County, California, U.S. Geological Survey open-file map; map scale 1:24,000.

Waring, G.A., 1919, Ground water in the San Jacinto and Temecula basins, California: U.S. Geological Survey Water-Supply Paper 429, 113 p.

White, D.E., 1983, Summary of hydrologic information in the El Paso, Texas, area, with emphasis on ground-water studies, 1903–1980: U. S. Geological Survey Open File Report 83-775, 77 p.

Wright, R.V., 1924, Report on agriculture, economic, and ground-water situation, Antelope Valley, California: Federal Land Bank of Berkeley, November 6, 1924, 115 p.

Yeats, R.S., 1983, Large-scale Quaternary detachments in the Ventura basin, southern California: Journal of Geophysical Research, v. 88, p. 569–583.

Zettlemoyer, B., 1990, 1988 annual water use-water supply balances: California Department of Water Resources Memorandum Report, 59 p.

Zohdy, A.A.R, and Bisdorf, R.J., 1990, Ground-water exploration using deep Schlumberger soundings at Edwards Air Force Base, California, Part I—Graham Ranch and Rogers Lake: U.S. Geological Survey Open-File Report 90-536, 95 p.

Zohdy, A.A.R., and Bisdorf, R.J., 1991, Ground-water exploration using deep Schlumberger soundings at Edwards Air Force Base, California, Part II—Rogers Lake and North of Edwards Air Force Base: U.S. Geological Survey Open-File Report 91-446, 109 p.

PWS-0196-0091